# N-glycosylation of the protein disulfide isomerase Pdi1 ensures *Ustilago maydis* virulence

Authors:

Miriam Marín-Menguiano¶, Ismael Moreno-Sánchez¶, Ramón R. Barrales, Alfonso Fernández-Álvarez* and José Ignacio Ibeas*

Centro Andaluz de Biología del Desarrollo (CABD), Universidad Pablo de Olavide-Consejo Superior de Investigaciones Científicas-Junta de Andalucía, Ctra. Utrera km.1, 41013 Seville, Spain.

¶ These authors contributed equally to this paper.

* Equal senior contribution; Correspondence: José Ignacio Ibeas (joibecor@upo.es) and Alfonso Fernández-Álvarez (aferalv@upo.es)

Short title: Pdi1 is required for full corn smut fungus virulence

## Abstract

Fungal pathogenesis depends on accurate secretion and location of virulence factors which drive host colonization. Protein glycosylation is a common posttranslational modification of cell wall components and other secreted factors, typically required for correct protein localization, secretion and function. Thus, the absence of glycosylation is associated with animal and plant pathogen avirulence. While the relevance of protein glycosylation for pathogenesis has been well established, the main glycoproteins responsible for the loss of virulence observed in glycosylation-defective fungi have not been identified. Here, we devise a proteomics approach to identify such proteins and use it to demonstrate a role for the highly conserved protein disulfide isomerase Pdi1 in virulence. We show that efficient Pdi1 N-glycosylation, which promotes folding into the correct protein conformation, is required for full pathogenic development of the corn smut fungus *Ustilago maydis*. Remarkably, the observed virulence defects are reminiscent of those seen in glycosylation-defective cells suggesting that the N-glycosylation of Pdi1 is necessary for the full secretion of virulence factors. All these observations, together with the fact that Pdi1 protein and RNA expression levels rise upon virulence program induction, suggest that Pdi1 glycosylation is a crucial event for pathogenic development in *U. maydis*. Our results provide new insights into the role of glycosylation in fungal pathogenesis.

## Author summary

Fungal pathogens require virulence factors to be properly secreted and localized to guarantee complete infection. In common with many proteins, virulence factors must be post-translationally modified by glycosylation for normal localization, secretion and function. This is especially important for virulence factors, which are mainly comprised of cell wall and secreted proteins. Aberrant glycosylation leads to a loss of virulence in both animal and plant pathogenic fungi. We have previously demonstrated that glycosylation is important for virulence of the corn smut fungus, *Ustilago maydis*. However, the glycoproteins involved and their specific roles in the infection process have not yet been reported. Here, we describe a proteomic assay designed to identify glycoproteins involved in plant infection. Using this method, we define the role of Pdi1 protein disulfide isomerase in virulence. Interestingly, abolishing Pdi1 N-glycosylation mimics Δ*pdi1* defects observed during infection, suggesting that Pdi1 N-glycosylation is required for the secretion of virulence factors. We hypothesize that Pdi1 N-glycosylation is crucial for maintaining proper effector protein folding during the infection process, especially in the harsh conditions found inside the maize plant.

## Introduction

Protein glycosylation is a common eukaryotic post-translational mechanism required for the correct folding, activity and secretion of many proteins. Glycosylation involves the synthesis and addition of different polysaccharide cores (sugars) to specific amino acids within a consensus sequence. Most glycoproteins are plasma membrane-associated cell wall and secreted proteins, which acquire glycosyl groups during their transit through the Endoplasmic Reticulum (ER) and Golgi Apparatus (GA) (1,2). Defects during the synthesis or addition of sugars to target proteins affect many biological processes; for instance, impaired human protein glycosylation causes more than 100 severe embryonic development disorders (3). In pathogenic fungi, glycosylation defects lead to a reduction or absence of virulence in plant and animal pathogens (4–8).

Protein glycosylation is divided into different types based on the structure and composition of the oligosaccharide cores and the amino acids to which they are attached. N- and O-glycosylation are the most common types in pathogenic fungi. N-glycosylation consists of the addition of an oligosaccharide core, composed of two N-acetylglucosamines (NAcGlc), nine mannoses (Man) and three glucose (Glc) molecules, $NAcGlc_2Man_9Glc_3$, to the nitrogen chain of an asparagine residue in the sequence Asn-*x*-Ser/Thr, where *x* can be any amino acid except proline (9,10). O-glycosylation is more variable than N-glycosylation in terms of the types of sugars added. In fungi O-mannosylation is the most common type of O-glycosylation and is characterized by the addition of Man residues to target proteins. In contrast to N-glycosylation, O-glycosylation involves sequential additions of Man to the

oxygen chain of Ser or Thr amino acids although no amino acid consensus sequence has been identified (11). N- and O- linked glycans are later processed during their transit across the ER and GA, and specific trimming of sugars is also essential for the function and secretion of glycoproteins (5,12).

Crucial components for fungal pathogenesis belonging to N- and O-glycosylation pathways have been identified in several organisms such as *Candida albicans*, *Aspergillus nidulans*, *Cryptococcus neoformans, Magnaporthe oryzae* or *Ustilago maydis* (4,6–8,13–15). The loss of these proteins primarily affects those stages of pathogenic development that require robust glycoprotein secretion. The involvement of protein glycosylation in fungal virulence has been extensively explored in the corn smut fungus *U. maydis* (4,5,16).

*U. maydis* combines both pathogenic and non-pathogenic life cycles. During the non-pathogenic cycle, *Ustilago* grows as haploid yeast-like cells that can be easily cultured in the laboratory. The pathogenic cycle starts when two sexually compatible strains mate on the maize plant surface. Sexual compatibility is determined by two independent loci: *locus a*, which encodes a pheromone-receptor system; and *locus b*, which encodes a transcription factor formed by a *bE/bW* heterodimer. Formation of the *bE/bW* complex triggers development of an infective dikaryon filament (17). Physical and chemical plant signals are sensed by filaments that develop a morphogenetic structure called the appressorium, which mediates plant cuticle penetration (18). Once inside plant tissues, the fungus expands in a branched filamentous form generating hypertrophied plant cells, macroscopically visible as tumors (19–23).

120 N- and O-glycosylation are both crucial for *U. maydis* pathogenic
121 development. The loss of the O-mannosytransferase Pmt4, which catalyzes
122 the addition of mannoses to target proteins, compromises both appressorium
123 formation and plant cuticle penetration. Hence, Δ*pmt4* cells are unable to
124 invade the plant tissues and tumor induction is fully abolished (4).
125 Glucosidase I and II (Gls1 and Gas1/Gas2) are important for N-glycan
126 processing in the ER and play crucial roles during the early stages of *U.*
127 *maydis* plant colonization (5,8). A reasonable explanation for these drastic
128 virulence defects is that deficient glycosylation could greatly alter the location
129 and/or function of glycoproteins involved in virulence, and consequently
130 compromise multiple stages of *U. maydis* pathogenic development such as
131 plant cuticle penetration, fungal progression inside plant tissues or plant
132 defense responses. Despite the importance of Pmt4 and Gls1 for maize
133 infection, the virulence factors glycosylated by these proteins are still poorly
134 described. In this context, an *in silico* search for putative Pmt4 targets
135 identified Msb2 as an O-glycoprotein, whose deletion causes virulence
136 defects that resemble some of those described for the Δ*pmt4* mutant (16).
137 However, a more wide-ranging approach is required to find new glycosylated
138 virulence factors.

139 In this work we devise a proteomics approach designed to identify N-
140 and O-glycoproteins produced when the infection program is activated. Using
141 this method, we identify several Gls1 and Pmt4 targets involved in virulence.
142 Among these, we further characterize Pdi1, a disulfide isomerase protein
143 whose glycosylation we demonstrate to be required for full virulence in maize
144 plants due to its involvement in glycoprotein folding. Furthermore, we show

that the deletion of Pdi1 affects glycoprotein secretion in *U. maydis*. We speculate about its role during the infection process, which could be related to ensuring the effective production and secretion of many virulence factors.

## Results

### Glycoproteomic screening for Pmt4 and Gls1 substrates

Previous work from our laboratory have shown that the *U. maydis* proteome contains a high number of putative O-glycoproteins mannosylated by the O-mannosyltransferase Pmt4 (16). An *in silico* screen for proteins harboring Ser/Thr-rich regions, where Pmt4 attaches mannoses, revealed that around 65% of *U. maydis* proteins are potential O-glycosylation targets (16). If proteins containing N-glycosylation sites are included, this number rises to over 70% of the proteome, suggesting a potential role for protein glycosylation in the activity of a high proportion of *U. maydis* proteins (Pérez-Pulido, personal communication). In order to identify virulence-related glycosylation targets, we designed a selective glycoproteomic screen based on the hypothesis that glycoproteins whose expression is modified upon virulence program induction are likely to have important roles in the pathogenic phase of the *U. maydis* life cycle.

For this screen we set out to analyze cell extracts corresponding to cytosolic, cell wall and secreted proteins using two-dimensional differential gel electrophoresis (2D-DIGE) to detect glycoproteins whose spot area or intensity were altered by the loss of Pmt4 or Gls1 and corresponding effect on O- or N- glycosylation activities, respectively. To isolate glycoproteins from

cytosolic extract and avoid interference with other proteins, total protein extracts were enriched for mannose-containing proteins by High-Performance Liquid Chromatography (HPLC) using *concanavalin A* columns (Fig 1). Due to the high proportion of glycoproteins in cell wall and secreted extracts, HPLC enrichment was not applied to these preparations. Entry into the virulence phase was controlled by expressing Biz1, a *b*-dependent zinc-finger protein whose induction activates pathogenic filamentous growth, under the control of the carbon source-regulated $P_{crg}$ promoter that is induced by arabinose (*biz ON*) and repressed by glucose (*biz OFF*) (24,25). Thus, wild-type (*wt*), Δ*pmt4* and Δ*gls1* cells harboring $P_{crg}$ controlled-*biz1* were collected under inducing and repressing conditions and protein samples compared, using three replicas of each, to identify the differentially migrating proteins (Fig 1).

By applying the approach described above, we detected protein spots whose areas showed altered electrophoretic mobility compared to *wt* in a Biz1-dependent manner in both Δ*pmt4* and Δ*gls1* cells, presumably corresponding to O- and N-glycoproteins, respectively. Using MALDI–MS we identified four proteins in the cytosolic extract with altered mobility in both mutants that probably correspond to both O- and N-glycosylated proteins: the chorismate mutase Cmu1, the α-L-arabinofuranosidase Afg1, the invertase Suc2 and Um10156, a putative disulfide-isomerase (Fig 2). In addition, we identified 27 N- or O-glycoproteins from the cytosolic extract, 6 from the cell wall extract and 11 from the secreted extract showing electrophoretic mobility changes (Fig 3, S1 Table). Of the proteins identified only Cmu1, Um04926 (Pep4), Afg1 and Um04309 (Afg3) have been previously characterized. Cmu1 is a secreted virulence factor that controls the metabolic status of plant cells

during fungal colonization; deletion of *cmu1* reduces *U. maydis* virulence in the solopathogenic strain CL13 (26). Pep4 is a proteinase A located at the vacuole, which is involved in the yeast to micelium dimorphic transition and whose deletion causes reduced virulence including incomplete teliospore maturation (27). On the other hand, Afg1 and Afg3 are arabinofuranosidases that participate in the degradation of arabinoxylan, a plant cell wall component. While the loss of *afg1* or *afg3* is dispensable for virulence, the triple deletion of *afg1, afg2* and *afg3* compromises full pathogenic development (28). The involvement of the other identified proteins in pathogenesis remains to be determined.

**The disulfide-isomerase Pdi1 is a substrate of Pmt4 and Gls1, and Pdi1 is required for pathogenesis**

To determine the involvement in pathogenesis of the uncharacterized proteins, we compared the virulence capability of CL13 strain mutants carrying deletions corresponding to several of the candidate proteins. The CL13 strain harbors genes encoding a compatible *bE1/bW2* heterodimer allowing it to complete full pathogenic development (29). Analysis of disease symptoms after infection revealed strong virulence defects in Δ*afg1,* Δ*Um00309*, Δ*Um02751*, Δ*Um03416*, Δ*Um04180*, Δ*Um04422*, Δ*Um04733*, Δ*Um05223*, Δ*Um10156,* and Δ*Um11496* infections (Fig 4A and S1 Table). Candidate genes were then tested in more virulent strains; the wild type FB1 and FB2 strains (30), which have a higher infection capacity, and SG200, which carries the *mfa2* gene that encodes the compatible mating type pheromone (29) and confers stronger virulence. Based on the virulence

assays in these backgrounds we identified Um10156 as having the most significant role in plant infection (Fig 4B, C and D). Blast analysis for Um10156 revealed 36% identity to *S. cerevisiae* Pdi1 with 48% and 43% identity in the two thioredoxin domains (Fig 5A and S1 Fig). Thus, we will now refer to Um10156 as Pdi1 for the remainder of the article. *S. cerevisiae* Pdi1 is a disulfide-isomerase protein, member of the thioredoxin superfamily of redox proteins whose canonical role is to support the folding of newly synthesized proteins in the ER *via* the addition of disulfide bonds (31).

**The loss of Pdi1 compromises fungal expansion inside plant tissues**

Previous studies in budding yeast have shown that Pdi1 function is critical under ER stress conditions, where a large number of misfolded proteins are produced (32,33). To confirm that this function of Pdi1 is retained in *U. maydis*, we explored Pdi1 localization and studied the ability of Δ*pdi1* cells to grow under reductive ER stress induced by DTT. Microscopy co-localization analysis of Pdi1:GFP and the ER marker mRFP:HDEL confirmed the localization of Pdi1 to this organelle (Fig 5B), where it has been shown to work in conjunction with Calnexin and Calreticulin in the refolding of glucosidated proteins (34). Moreover, Δ*pdi1* cells showed a hypersensitivity response to DTT, thus confirming the canonical role of Pdi1 in *U. maydis* (Fig 5C and D).

To identify the causes behind the failure of Δ*pdi1* plant infections we first analyzed if the *pdi1* deletion causes growth alterations under axenic conditions. We found no differences in generation time (~2.5 hours in rich media) (S2A Fig) or cell morphology (S2B Fig) between *wt* and Δ*pdi1* cells.

Moreover, Δ*pdi1* did not show any defects in cell wall integrity or oxidative stress resistance (S3 Fig). Next, we examined if the mating capability between sexually compatible cells depends on Pdi1. This can be tested by analyzing dikaryon filament formation on charcoal plates, which are recognizable by the formation of white fuzzy colonies. We observed similar mating efficiency in FB1Δ*pdi1* and FB2Δ*pdi1* crosses compared to the *wt* strains (Fig 6A). Therefore, the pathogenic defects affecting Δ*pdi1* infections are probably not caused by failures in cellular growth or mating stages. Hence, the plant infection defects observed in *pdi1* mutant cells probably appear during interaction with the host. In fact, we have observed an increase in both Pdi1 protein levels upon *biz1* activation and *pdi1* transcription during the infection process, with a peak at three days post infection (Fig 7), in agreement with a high-throughput transcriptomic analysis of pathogenesis (35). These observations suggest that Pdi1 function is required during the plant infection process, possibly to ensure the correct folding of the increased quantity of glycosylated and secreted proteins that must be expressed for a successful infection to develop.

To determine which step of *U. maydis* pathogenic development is affected by the loss of Pdi1, we analyzed the behavior of Δ*pdi1* cells during plant cuticle pre-penetration stages. A physicochemical plant signal is recognized by the fungal cell, triggering filamentous growth and appressoria formation (18). In order to quantify both phenotypes, we generated the *pdi1* deletion in SG200 cells carrying RFP under the control of the constitutive *otef* promoter and co-inoculated maize plants with an equal mixture of SG200 $P_{otef}$GFP and SG200 $P_{otef}$RFP Δ*pdi1* cells. The amount of filaments and

appressoria in *wt* and Δ*pdi1* cells was quantified using fluorescence microscopy ~15 hours after infection. We found that the absence of Pdi1 did not alter filament formation capability (Fig 6B). Moreover, Δ*pdi1* filaments developed appressoria normally (Fig 6C). Thus, plant penetration stages do not require Pdi1, which suggests that deficient fungal expansion inside plant tissues might be behind the Δ*pdi1* infection defects.

To address the state of fungal colonization inside plant tissues we stained infected maize leaves 3 and 5 days after inoculation using WGA-Alexa and propidium iodide to visualize fungal hyphae and plant cells, respectively (see Methods). Following this approach, we observed a defective proliferation of Δ*pdi1* hyphae inside the plant (Fig 6D). To confirm these observations, we quantified fungal biomass in plant samples. We used the expression level of the *U. maydis ppi1* gene as a fungal marker (36). We found that the amount of fungal biomass 3 days post-infection decreased two-fold during Δ*pdi1* infection versus infection with a *wt* strain (Fig 6E). Thus, Pdi1 plays a key role in *U. maydis* colonization after plant penetration. Interestingly, this phenotype is reminiscent of defects caused by N-glycosylation defective cells (5) suggesting that altered Pdi1 function might be partly responsible for the defects associated with the loss of N-glycosylation.

**Loss of Pdi1 N-glycosylation mimics Δ*pdi1* virulence defects**

An important remaining question is whether the loss of Pdi1 glycosylation mediated by Pmt4 and Gls1 leads to dysfunctional Pdi1 and a reduction in virulence similarly to Δ*pdi1* cells, or alternatively, a non-glycosylated Pdi1 form is still able to induce plant tumors and Pmt4 and Gls1

affect virulence elsewhere. To address this issue, putative O- and N-glycosylation sites were substituted with alanine (S4A, S24A, S340A, S344A, S346A, S350A, S477A and T486A) and glutamine (N36Q and N484Q) residues, respectively (Methods, Fig 8A). Pdi1 alleles harboring substitutions at all O-glycosylation sites (Pdi1$^{\Delta O\text{-}gly}$), all N-glycosylation sites (Pdi1$^{\Delta N\text{-}gly}$), all O- and N-glycosylation sites (Pdi1$^{\Delta N,O\text{-}gly}$) or the wild type allele were introduced in the exogenous *ip* locus of Δ*pdi1* cells under the control of the *otef* promoter and their ability to infect maize plants tested. We found that while Pdi1$^{\Delta O\text{-}gly}$ restored the virulence defects observed in Δ*pdi1* cells during infection similar to the *wt* allele, Pdi1$^{\Delta N\text{-}gly}$ and Pdi1$^{\Delta N,O\text{-}gly}$ forms failed to complement the lack of Pdi1 (Fig 8B). This strongly suggests that only the N-glycosylation of Pdi1 is relevant for its role in virulence. Similarly to Δ*pdi1* cells, the virulence defects observed in Pdi1$^{\Delta N\text{-}gly}$, are due to a failure in the fungal expansion inside the plant tissues (Fig 8C). Remarkably, Pdi1$^{\Delta N\text{-}gly}$ could be detected by western blot discarding a possible degradation of Pdi1 in the absence of proper N-glycosylation (Fig. 8D). Consistent with defective Pdi1 function during plant infection when N-glycosylation target residues are removed, we observed that Pdi1$^{\Delta N\text{-}gly}$ does not complement the DTT sensitivity shown by the Pdi1 deletion mutant (Fig 8E).

**Δ*pdi1* and Δ*gls1* show similar secreted protein defects**

Taking our results together with the established functions of Pdi1 in other model organisms lead us to propose a model whereby Gls1-mediated glycosylation of Pdi1 is required for correct folding and subsequent secretion of proteins activated by the virulence program. To explore this hypothesis, we

compared the secretomes of *wt*, Δ*pdi1* and Δ*gls1* cells upon Biz1 induction (pathogenic filamentous growth) conditions. We found 6 secreted proteins showing differential electrophoretic mobility in *wt versus* Δ*pdi1* cells: Um06158 (probable glutaminase A), Um01829 (Afg1, previously identified in our first screening, see Fig 1), Um04503, an α-N-acetylgalactosaminidase, and Um01213, Um00027 and Um11462 (3 uncharacterized proteins) (see Fig 9). Remarkably, 4 out of these 6 proteins (Um06158, Um01829, Um04503 and Um00027) were also identified in the comparison between *wt* and Δ*gls1* secretomes suggesting that the effects caused by Δ*gls1* might be explained by deficient Pdi1 function. This indicates that there is a pool of secreted proteins that are glycosylated by Gls1 and their proper folding is dependent on Pdi1, which itself requires Gls-mediated glycosylation for function. The fact that the number of glycoproteins altered by the loss of *gls1* is higher than by *pdi1* is probably because a group of N-glycoproteins does not require Pdi1 for correct folding, secretion and function. This is consistent with the fact that Δ*gls1* causes more severe virulence defects than Δ*pdi1* (See model Fig 10).

## Discussion

In this work, we have demonstrated that the use of glycosylation mutants Δ*pmt4* (4) and Δ*gls1* (5) in a virulence program-specific 2D-DIGE protein analysis is a suitable and effective approach for identifying *Ustilago maydis* glycoproteins involved in plant infection. We identified 35 glycoproteins, and showed that 14 out of the 28 (50%) assayed are involved

in virulence, analyzing single deletion mutants. Of these mutants, loss of the protein disulfide isomerase Pdi1 had the strongest effect on virulence, most likely due to protein folding defects and changes in functionality and/or secretion of proteins required for plant infection.

**An effective method for identifying new glycosylated fungal effectors**

It is well established that protein glycosylation is essential for fungal infection. Mutants for specific glycosyltransferases or glycosidades are affected at different stages of the infection process in *Ustilago maydis* (4,5), other plant pathogens such as *Penicilium digitatum* (37), *Margnaporthe oryzae* (15,38) and *Botrytis cinerea* (39) as well as in animal pathogens such as *Candida albicans* (13,40) and *Cryptococcus neoformans* (6,41,42). Thus, our interest focused on determining which of the glycosylated proteins produced during the infection process were responsible for those defects. We postulated cell wall and secreted proteins as the main sources of novel virulence factors. Cell wall proteins form the pathogen's most external layer while secreted factors have well established roles as effector proteins (43). Significantly, almost all cell wall and secreted factors are glycosylated (44,45). *U. maydis* putatively secretes 467 effectors that contribute to the establishment of biotrophy with maize during the infection process (19,22). In-silico tools such as SignalP (46), ApoplastP (47) or EffectorP (48) can predict which proteins are secreted and could be putative effectors. Although useful guides, such bioinformatic tools are not completely reliable since it has also been demonstrated that some fungal effectors are not secreted through the canonical secretion pathway involving N-terminal signal peptide degradation

prior to translocation to the ER (49–52). For example, while around 90% of proteins secreted by *Fusarium graminearum* in axenic culture possess a signal peptide, only 56% of proteins secreted during the infection process have secretion signals (53). Different strategies such as RNA-seq and microarray, have been employed in *Ustilago maydis* in order to identify effectors whose transcription is induced during infection (54–57). Such studies highlight the huge changes in gene expression that occur during different stages of the infection process. Nevertheless, none of these approaches took into consideration the importance of protein modification, which are especially important for secreted proteins. For this reason, a proteomics approach can be an attractive alternative to identify proteins with important roles in the plant infection process. Hence, in this work we established a new approach to identify glycosylated effectors based on their electrophoretic mobility. Alterations to the glycosylation status of a protein in O- or N-glycosylation mutant strains, Δ*pmt4* or Δ*gls1* respectively, can be detected by bidimensional gel electrophoresis. This strategy allowed us to identify 27 glycoproteins from the cytosolic extract, 11 from the secreted protein extract and 6 from the cell wall extract, with some detected in multiple extracts. It is important to highlight that this approach identified previously characterized proteins involved in virulence as well as known effectors such as Afg1 and Afg3 (28), Pep4 (27) and Cmu1 (26). Among the 35 proteins identified, 4 are cell wall proteins that could be related to plant interaction during infection and 18 are located (Djamei, personal communication) and/or predicted to be located at the apoplastic region (S1 Table), which is consistent with effector protein function. Similar proteomic strategies based

394 on glycosylation changes after the activation of virulence programs have been
395 used to identify new fungal effectors in other pathogenic fungi. For example,
396 the controlled induction of Mst11, a *Magnaporthe oryzae* MAP kinase
397 essential for appressoria formation and plant infection (58) has been assayed
398 in O-glycosylation mutants such as Δ*MoPmt2* (38) and Δ*MoPmt4* (59), as well
399 as in N-glycosylation mutants such as Δ*alg3* (15) and Δ*Mogls2* (60).
400 Although it has been described that many single effector gene
401 deletions do not affect plant infection (22), half of the glycoprotein deletions
402 examined in a CL13 background showed a reduction in the number or size of
403 tumors when maize plants were infected (Fig 4). In fact, 14 of the 28 single
404 deletion mutants assayed showed a statistically significant decrease in the
405 number of tumors. Interestingly, four of these deletions induced only very
406 small (<1 mm) tumors. Ten of the most promising candidates were then
407 deleted in the SG200 strain and tested for virulence in maize plants, showing
408 that *Δpdi1* was the least virulent mutant. Single deletions for the other genes
409 in this background caused little or no reduction in virulence. This observation
410 may be explained by the fact that the CL13 strain does not possess the
411 pheromone encoding gene *mfa2* (29) resulting in a reduced ability to develop
412 filaments and produce tumors during maize plant infection. Thus, CL13 is
413 more sensitive to the deletion of genes with minor but important contributions
414 to the infection process.
415 Total disruption of the whole glycosylation process in *U. maydis* leads
416 to avirulent phenotypes because of its inability to develop functional
417 appressoria (Δ*pmt4*) or due to failure to spread inside the maize plant (Δ*gls1*)
418 (4,5,61), however we did not find a single factor which resembles these

419 phenotypes. The reason why this single factor was not identified might be
420 because *U. maydis* instead uses a pool of glycosylated effectors that work
421 cooperatively to perform the different steps involved in plant invasion and
422 colonization.
423
424 **Pdi1 is a key factor supporting *U. maydis* pathogenic development**
425 Of all the virulence-related glycoproteins identified here, we chose to
426 further characterize Pdi1 as its deletion led to the strongest reduction in
427 virulence. As we expected, Pdi1 localized to the ER and its deletion led to
428 growth defects in axenic culture when an ER stress-inducing drug such as
429 DTT was added to either solid or liquid media (Fig 5). These results support
430 the idea that Pdi1 is a disulfide-isomerase protein that might assist the folding
431 of newly synthetized proteins in the ER *via* the addition of disulfide bonds,
432 which is critical during ER stress conditions (33). Many *U. maydis* effector
433 proteins harbor cysteine-rich regions suitable for the formation of disulfide
434 bonds, which may be necessary for their acquisition of active conformations
435 (22,62,63). Thus, Pdi1's role in establishing disulfide bonds in proteins
436 involved in plant infection could be a major part of how the Δ*pdi1* mutation
437 affects virulence. Moreover, both calreticulin (CRT) and calnexin (CNX),
438 which bind glycosylated N-glycans in the ER, have a Pro-rich arm that may
439 bind a protein disulfide isomerase (34), such as Pdi1. N-glycans may also
440 play an important role in ER-associated degradation (ERAD) of proteins (34).
441 Consequently, Pdi1 may be directly or indirectly involved in the selection of
442 misfolded glycoproteins for dislocation into the cytosol for degradation by
443 proteasomes, i.e., through N-glycans and mannosidase 1 (Mns1) and a

444 second set of proteins called MnlI (mannosidase-like), Htm1 (homologous to
445 mannosidase), or ER degradation-enhancing α-mannosidase-like protein
446 (EDEM) (1,34,64,65).

447 We have demonstrated that the Pdi1 deletion strain can complete the
448 initial steps of the infection process, appressoria formation and dikaryotic
449 filament formation normally (Fig 6). Inside the maize plant, this mutant is able
450 to form clamp-like cells and hyphae spread into maize cells although it cannot
451 reach the vascular tissue. This growth defect was also observed by qPCR
452 fungal biomass quantification, with more than a 50% reduction in fungal
453 biomass versus wild-type (Fig 6). During *U. maydis* biotrophic development
454 until tumor formation at 6 dpi, the fungus has to form the dikaryotic filament,
455 develop appressoria, penetrate into the plant, modify plant metabolism to
456 avoid activation of the plant's immune system and ensure its proper
457 propagation inside the host. In order to achieve all these tasks, *U. maydis*
458 secretes several early effectors such as Pep1 (66,67), Pit2 (68), Stp1 (35)
459 and See1 (69). As Δ*pdi1* did not show any defects in appressoria formation,
460 dikaryotic filament formation or maize plant penetration, the reduction in
461 fungal biomass observed in this mutant may be the result of a failure of the
462 folding and secretion of proteins to the apoplast. Therefore, we propose three
463 non-mutually exclusive mechanisms by which the loss of Pdi1 could affect
464 fungal virulence: 1) a decrease or abolition in the secretion of effectors; 2) a
465 reduction or elimination of the activity of the secreted effectors; 3) the
466 presence of abnormally folded proteins that behave as new pathogen-
467 associated molecular patterns (PAMPs) and activate the plant immune
468 system. Work towards deciphering the molecular basis of Pdi1 action during

plant infection and testing the above hypotheses is currently ongoing in our laboratory. Our results raise the possibility that mechanisms linking glycosylation and disulfide bond formation of fungal effectors are conserved and highlight the need to explore Pdi1's role in other fungal pathogens.

## Abbreviations

ER: Endoplasmic Reticulum

GA: Golgi Apparatus

DIGE: Differential in Gel Electroforesis

HPLC: High Performance Liquid Chromatography

DTT: Dithiothreitol

MALDI-MS: Matrix-Assisted Laser Desorption/Ionization – Mass Spectrometry

ERAD: ER-Associated Degradation

dpi: days post-infection

PAMPs: Pathogen-Associated Molecular Patterns

CWP: Cell Wall Protein

IEF: Isoelectric Focusing

## Acknowledgements

We thank Antonio Pérez-Pulido for help with the *in silico* screening of glycosylation sites, Armin Djamei for sharing data about apoplastic proteins, and John R. Pearson for critical comments on the manuscript. We would like to thank the Genetics Department for their useful discussions and comments, Víctor Manuel Carranco for the graphic design in the figures and Sandra Romero for technical support. MMM was supported by P09- AGR-5241 Junta

de Andalucía. IMS was awarded by BES-2014-069149 MINECO AEI/FEDER, UE, Spain. This work was supported by Junta de Andalucía P09- AGR-5241 grant and Spanish Government BIO2013–48858-P and BIO2016-80180-P grants from MINECO AEI/FEDER, UE and Ramon y Cajal program, RyC-2016-19659 to AFA.

## Materials and Methods

### Strains, plasmid and growth conditions

*Escherichia coli* DH5α and pGEM-T easy (Promega) and pJET1.2/blunt (ThermoFisher Scientific) were used for cloning purposes. Growth conditions for *E. coli* (70) and *U. maydis* (71) have been previously described. *U. maydis* strains used in this study are listed in S2 Table.

To induce the over-expression of transcription factor Biz1 (25), FB1Biz1$^{crg}$ and its derivative mutants (FB1Biz1$^{crg}\Delta$*pmt4*, FB1Biz1$^{crg}\Delta$*gls1* and FB1Biz1$^{crg}\Delta$*pdi1*) cells were grown at 28ºC in complete medium (CM) supplemented with D-glucose 25% (CMD), washed twice with water and grown in CM supplemented with arabinose 25% (CMA) at 28ºC for 8 hours.

Pathogenicity assays were performed as described in (19). *U. maydis* cultures were grown at 28ºC to exponential phase in liquid YEPSL (0.4% bactopeptone, 1% yeast extract and 0.4% saccharose) and concentrated to an $OD_{600}$ of 3, washed twice in water and injected into 7 days old maize (*Zea mays*) seedlings (Early Golden Bantam). Disease symptoms were quantified 14 dpi. Statistical analyses were performed in GraphPad Prism 6 software.

518 ER stress assays were carried out with cultures grown at 28 ºC to exponential
519 phase in CMD and spotted at 0.4 $OD_{600}$ onto CM plates supplemented with 4
520 mM DTT (iNtRON Biotechnology). Plates were incubated for 48 h at 28 ºC.
521 For ER stress assay in liquid culture, *U. maydis* cells were grown to
522 exponential phase in YEPSL and diluted to 0.1 $OD_{600}$ in YEPSL with 10 mM
523 DTT. Cell growth at 28 ºC with continuous shaking was analyzed over 24 h
524 using a Spark 10M (Tecan) fluorescence microplate reader.
525 Cell wall integrity and oxidative stress assays were carried out with cultures
526 grown at 28 ºC to exponential phase in CMD and spotted at 0.4 $OD_{600}$ in CM
527 plates supplemented with calcofluor white 40 µg/ml (Sigma-Aldrich), Congo
528 Red 50 µg/ml (Sigma-Aldrich), Tunicamycin 1 µg/ml (Sigma-Aldrich), Sorbitol
529 1M (Sigma-Aldrich), 2% DMSO (Sigma-Aldrich), $H_2O_2$ 1.5 mM (Sigma-
530 Aldrich) and NaCl 1M (Sigma-Aldrich). Plates were incubated for 48 h at 28
531 ºC.
532 For mating and filamentation assays, cells were grown in liquid YEPSL until
533 exponential phase, washed twice with sterile bidistilled water, spotted onto
534 PD-charcoal plates and grown for 24-48 hours at 25-28ºC.
535
536 **DNA and RNA procedures**
537 Molecular biology techniques were used as described in (70). *U. maydis* DNA
538 isolation and transformation were carried out following the protocol described
539 in (72).
540 To generate deletion mutants, 1 kb fragments of the 5' and 3' flanks of the
541 gene of interest (*goi*) ORF were generated by PCR using Phusion High
542 Fidelity DNA polymerase (New England Biolabs) or Q5 High-Fidelity DNA

polymerase (New England Biolabs) and *U. maydis* FB1 genomic DNA, using the primers *goi*KO5-1 and *goi*KO5-2 (containing a *SfiI* restriction site) to amplify the 5' flank and *goi*KO3-1 (containing a *SfiI* restriction site) and *goi*KO3-2 to amplify the 3' flank (S3 Table). These fragments were digested with *SfiI* and ligated with the 1.9-kb *SfiI* carboxin, 1.4-kb *SfiI* noursethricin (*ClonNAT*), 2-kb *SfiI* geneticin or 1.9-kb *SfiI* hygromicin resistance cassettes (73). Constructs were cloned into pGEM-T easy (Promega) or pJET1.2/blunt (ThermoFisher Scientific) plasmids and amplified by PCR using the primers *goi*KO5-1/*goi*KO3-2, prior to their transformation in *U. maydis*.

To generate SG200 2xRFPΔ*pdi1* used for filament quantification into the maize plant, pGEM-TΔ*pdi1:cbx* plasmid was digested with *SfiI* to excise the carboxin resistance cassette and ligated to a hygromicin resistance cassette isolated from pMF1h (73) with *SfiI*/*BsaI* double digestion, leading to pGEM-TΔ*pdi1:hyg*. This construct was amplified by PCR with Phusion DNA polymerase using primers pdi1KO5-1/pdi1KO3-2 and integrated into the SG200 2xRFP strain (74).

For the SG200 3xGFP strain used for filament quantification in planta, the pOG plasmid (74), containing 3xGFP under the control of the *otef* promotor and a hygromicin resistance cassette, was digested with *PsiI* and integrated into the SG200 strain. Finally, Δ*pdi1:cbx* was amplified by PCR using primers pdi1KO5-1/pdi1KO3-2 and integrated into the SG200 3xGFP strain.

To perform *pdi1* deletion complementation assays, we generated the SG200Δ*pdi1*$P_{otef}$*pdi1* strain. To this end, the eGFP fragment in p123 (75) was substituted with the *pdi1* ORF. The *pdi1* ORF was amplified by PCR using

567 Phusion HF DNA polymerase (New England Biolabs) with primers
568 pdi1StartXmaI and pdi1StopNotI, containing XmaI and NotI restriction sites,
569 respectively. The PCR product was digested with XmaI and NotI, purified and
570 cloned into the p123 plasmid digested with both restriction enzymes, creating
571 p123-*pdi1*. Finally, p123-*pdi1* was linearized with *SspI* and integrated into the
572 SG200Δ*pdi1 ip* locus by homologous recombination.
573 To create an O-glycosylation deficient *pdi1* mutant, serine or threonine sites
574 predicted by NetOgly 4.0 tool were replaced by site-direct mutagenesis using
575 GenScript (Piscataway, USA), generating the plasmid pUC57-*pdi1*mutO-gly,
576 with *Sma1* and *NotI* restriction sites. The *pdi1*mutO-gly construct was
577 reintroduced into p123 as described above, creating the p123-*pdi1*mutO-gly
578 vector. This plasmid was linearized with *SspI* and integrated into the
579 SG200Δ*pdi1 ip* locus by homologous recombination, generating the
580 SG200Δ*pdi1pdi*$^{\Delta O\text{-}gly}$ strain.

581 To generate an N-glycosylation mutant version of *pdi1*, asparagine 36 and
582 484 were replaced by glutamine in N-glycosylation sites through PCR using
583 the Gibson Assembly® Cloning Kit (New England BioLabs, Frankfurt,
584 Germany) with primers PDI1Asn36mut-1 and PDI1Asn36mut-2 for the
585 mutation N36Q and primers PDI1Asn484mut-1 and PDI1Asn484mut-2 for the
586 mutation N484Q, using p123-*pdi1* as template, generating the plasmid p123-
587 *pdi1*mutN-gly. This construction was integrated into the SG200Δ*pdi1 ip* locus
588 (as described above), leading to SG200Δ*pdi1pdi*$^{\Delta N\text{-}gly}$ strain.

589 To generate the O- and N-glycosylation *pdi1* mutant, N36 and N484 was
590 replaced by glutamine using PCR and the Gibson Assembly Cloning Kit, with

primers PDI1Asn36mut-1/PDI1Asn36mut-2 for the N36Q mutation and PDI1Asn484mutThr486mut-1/PDI1Asn484mutThr486mut-2 for the N484Q mutation, and the plasmid p123-*pdi1*mutO-gly as template, reintroduced into p123 to generate p123-*pdi1*mutN,O-gly. This construct was linearized with *SspI* and reintegrated into the SG200Δ*pdi1 ip* locus.

All *pdi1* mutants for N- and/or O-glycosylation were confirmed by sequencing, using primers PDI1SeqI and PDI1SeqII.

For GFP tagging of *pdi1*, we generated plasmid pDL51-*pdi1*. This plasmid is a p123 derivative (16) where *pdi1* ORFs were PCR amplified using Phusion DNA polymerase with primers pdi1ORF5/pdi1ORF3, was cloned in frame with the GFP present in the plasmid, under the control of the constitutive expressed *otef* promotor. To achieve this, pDL51 was linearized with *SfiI* digestion and ligated with the *pdi1* ORF digested with *SfiI*. For GFP tagging of the N-glycosylation mutant version of PDI1, *pdi1*mutN-gly was amplified by PCR with primers pdi1StartXmaI and pdi1StopNcoI containing XmaI and NcoI restriction sites, respectively. The PCR product was digested with XmaI and NcoI, purified and cloned into the p123GFP plasmid digested with both restriction enzymes, to generate an in frame C-terminal *pdi1*mutN-gly GFP fusion. Finally, p123-*pdi1*mutN-glyGFP was linearized with *SspI* and integrated into the SG200Δ*pdi1 ip* locus by homologous recombination.

For fungal biomass quantification, 3 and 5 dpi maize leaves were ground in liquid nitrogen and total DNA was isolated with DNeasy Plant Mini kit (Qiagen) according to manufacturer's instructions. Fungal biomass was then quantified by Real-Time PCR with an ABIPRISM 7000 Sequence Detection System (Applied Biosystems) using the Power SYBR Green PCR Master Mix

(ThermoFisher Scientific) according to the manufacturer's protocol, measuring the constitutively-expressed fungal *ppi1* gene, using primers RT-PPI1-5/RT-PPI1-3, and and constitutively-expressed plant *gapdh*, using primers Gapdh-F/Gapdh-R for normalization purposes. 100 ng of total DNA was used a template for each reaction.

For Pdi1 expression analysis, RNA from FB1 axenic culture and maize plants infected with FB1 and FB2 was isolated at 1, 3, 5 and 9 dpi, ground in liquid nitrogen using a pestle and mortar and purified using TRIzol reagent (Thermo Fisher Scientific) and the Direct-zol™ RNA Miniprep Plus kit (Zymo Research), following the manufacturer's instructions. cDNA was synthetized using RevertAid H Minus First Strand cDNA Synthesis kit (Thermo Fisher Scientific) following the manufacturer's instructions. Pdi1 expression levels were quantified by qRT-PCR using a Real-Time CFX Connect (Biorad) and SYBR® Premix Ex Taq™ II (Tli RNase H Plus) (Takara) according to the manufacturer's protocol, measuring *pdi1* expression gene, using primers pdi1 RT-fwd/pdi1 RT-rev, and *ppi1* as a constitutively-expressed control, using primers RT-PPI1-5/RT-PPI1-3.

**Proteomic analysis**

To detect pathogenesis-related changes to the cytosolic proteome caused by the loss of *pmt4*, we isolated O-glycosylated proteins from FB1Biz1$^{crg}$ and FB1Biz1$^{crg}\Delta$*pmt4* strains. FB1 and FB1Δ*pmt4* strains were used as controls. Cells from each strain were grown in 1 L of CMD to an $OD_{600}$=0.5-0.8, washed twice with sterile bidistilled water and grown for 8 hours in 1 L of CMA. After filamentation induction, samples were harvested by centrifugation,

641 washed twice in ice-cold 20 mM Tris-HCl buffer (pH 8.8) and frozen at –80 ºC.
642 Cells were then resuspended in lysis buffer (20 mM Tris-HCl, 0.5 M NaCl, pH
643 7.4) containing protease inhibitor cocktail (cOmplete Tablets, EDTA-free,
644 Roche) after which cell lysis was performed using glass beads (Sigma) in a
645 FastPrep®-24 homogeniser (MP Biomedicals), with power set to 6.0 using 3 x
646 45" pulses at maximum speed with 5 min rest between cycles. After cell lysis,
647 tubes were drilled with a needle and put into a new tube and samples were
648 recovered by centrifugation at 4000 rpm for 1 min. Subsequently, samples
649 were centrifuged at 14000 rpm for 30 min at 4ºC and the supernatant was
650 collected. One volume of 2x binding buffer (20 mM Tris-HCl, 0.5 M NaCl, 2
651 mM $MnCl_2$, 2 mM $CaCl_2$, pH 7.4) was added and concentrated using Amicon
652 Ultra-15 3 kDa centricon (Merk Millipore) and O-glycosylated proteins isolated
653 by affinity chromatography using Concavaline A columns (HiTrap Con A 4B,
654 GE Healthcare) in AKTA FPLC (GE Healthcare), and eluted with a buffer
655 containing 20 mM Tris-HCl, 0.5 M NaCl and 0.5 M methyl-α-D-
656 manopyranoside (pH 7.4).
657 To detect pathogenesis-related changes to the cytosolic proteome caused by
658 the loss of *gls1*, FB1Biz1$^{crg}$ and FB1Biz1$^{crg}\Delta$*gls1* cells were grown in 1 L of
659 CMD to an $OD_{600}$=0.5-0.8, washed twice with sterile distilled water and grown
660 for 8 hours in 1 L of CMA. FB1 and FB1Δ*gls1*, used as controls, were grown
661 in 2 L of CMD to an $OD_{600}$=0.5-0.8, washed twice with sterile distilled water
662 and grown during 8 hours in 2 L of CMA. Samples were harvested by
663 centrifugation, washed twice in ice-cold 20 mM Tris-HCl buffer (pH 8.8) and
664 frozen by dropping samples in liquid nitrogen. Cells were lysed with 3-4 cycles
665 in 6870 Freezer/Mill (SPEX, SamplePrep) according to the manufacturer's

instructions. Samples were resuspended in binding buffer (20 mM Tris-HCl, 0.5 M NaCl, 2 mM $MnCl_2$, 2 mM $CaCl_2$, pH 7.4) containing protease inhibitor cocktail (cOmplete Tablets, EDTA-free, Roche) and centrifuged at 14000 rpm for 30 min at 4ºC. Supernatant was filtered and N-glycosylated proteins isolated by affinity chromatography using Concavaline A columns (HiTrap Con A 4B, GE Healthcare) in AKTA FPLC (GE Healthcare), and eluted with a buffer containing 20 mM Tris-HCl, 0.5 M NaCl and 0.5 M methyl-α-O-glucopyranoside (pH 7.4).

For differential analysis of secreted O- or N-glycoproteins in Δ*pmt4* or Δ*gls1* mutants, FB1Biz1$^{crg}$ and FB1Biz1$^{crg}$Δ*pmt4* or FB1Biz1$^{crg}$Δ*gls1* cells were grown in 1 L of CMD to an $OD_{600}$=0.5-0.8, washed twice with sterile bidistilled water and grown for 8 hours in 1 L of CMA. After filamentation induction, cells were centrifuged, the supernatant filtered and secreted glycosylated proteins precipitated with deoxycholate acid and TCA.

Cell wall O- or N-glycoproteins in Δ*pmt4* or Δ*gls1* mutants were purified following the protocol described in (76), with some modifications. FB1Biz1$^{crg}$ and FB1Biz1$^{crg}$Δ*pmt4* or FB1Biz1$^{crg}$Δ*gls1* cells were grown in 1 L of CMD to an $OD_{600}$=0.5-0.8, washed twice with sterile bidistilled water and grown for 8 hours in 1 L of CMA. After filamentation induction, samples were harvested by centrifugation, washed four times in ice-cold 10 mM Tris-HCl buffer (pH 7.4) and frozen at –80 ºC. Cells were then resuspended in 10 mM Tris-HCl buffer (pH 7.4) containing protease inhibitor cocktail (cOmplete Tablets, EDTA-free, Roche) after which cell lysis was performed with glass beads (Sigma) in a FastPrep®-24 homogeniser (MP Biomedicals), with power set to 6.5 using 6 x

690 60" pulses at maximum speed with 3 minutes rest between cycles. Samples
691 were recovered by centrifugation at 3000 x g for 10 min at 4ºC, after drilling
692 the bottom of the tube with a needle and placing into a new tube. The pellet
693 (cell wall) was collected and washed sequentially with ice-cold sterile
694 bidistilled water, 5% NaCl with protease inhibitor, 2% NaCl with protease
695 inhibitor and 1% NaCl with protease inhibitor. Washing steps were repeated
696 three more times and cell wall proteins (CWPs) purified after 10 min at 100 ºC
697 in extraction buffer (50 mM Tris-HCl pH 8.0, 100 mM EDTA, 2% SDS, 10 mM
698 DTT) followed by 15 min centrifugation at 35000 x g. CWPs were then
699 collected from the supernatant.
700 To analyze the common target between Gls1 and Pdi1, secreted proteins
701 from FB1Biz1$^{crg}$ and FB1Biz1$^{crg}\Delta$*gls1* or FB1Biz1$^{crg}\Delta$*pdi1* were precipitated
702 with deoxycholate acid and TCA following the protocol described above for
703 secreted O- and N-glycoproteins.
704 Isolated proteins for each fraction and genotype were then precipitated with
705 2D Clean-Up kit (GE Healthcare), and dissolved in TS buffer (7M urea, 2M
706 thiourea, and 4% CHAPS) containing 30 mM Tris-HCl (pH 9.5). Protein
707 concentration was determined using RC DC Protein Assay (Bio-Rad).
708 Fifty micrograms of protein extract from each sample were labeled with Cy3-
709 or Cy5 Dye (GE Healthcare). Labeling was performed reciprocally so that
710 each sample was separately labeled with Cy3 and Cy5 to account for any
711 preferential protein labeling by the CyDyes. Twenty-five micrograms of each
712 sample were labeled with Cy2-Dye and pooled together as an internal
713 standard. Labeling was performed according to the manufacturer's
714 instructions. Different IEF procedures were performed. For cytosolic O-

715 glycoproteins and CWPs, IEF was performed in 24 cm 4–7 NL Immobiline
716 DryStrip (GE Healthcare) in an IPGphor unit (GE Healthcare) at 20 ºC as
717 follows: rehydratation for 12 h, 500 V for 1 h, linear gradient from 500 to 1000
718 V for 1 h, linear gradient from 1000 to 8000 V for 3 h and 8000 V to 60000
719 total Vhr for 5.5 h. The same IEF procedure using 24 cm 3-10 NL DryStrips
720 was performed for secreted proteins. For cytosolic N-glycoproteins, IEF was
721 performed using 24 cm 3–7 NL Immobiline DryStrip (GE Healthcare) in an
722 IPGphor unit (GE Healthcare) at 20 ºC as follows: rehydration for 12 h, 500 V
723 for 1.5 h, linear gradient from 500 to 1000 V for 7 h, linear gradient from 1000
724 to 8000 V for 8 h and 8000 V to 60000 total Vhr for 5.5 h. After IEF, strips
725 were incubated for 15 min at room temperature in a shaker in equilibration
726 buffer (50 mM Tris-HCl [pH 8.5], glycerol 30% v/v, 6M urea, 2% w/v SDS) with
727 10 mg/mL DTT, followed by another 15 min incubation in equilibration buffer
728 with 25 mg/mL iodoacetamide and loaded onto 10% acrylamide gels. Second
729 dimension separation was performed using an EttanDalt Six Electrophoresis
730 Unit (GE Healthcare).
731 After electrophoresis, gels were imaged using a Typhoon-9400 scanner (GE
732 Healthcare) with a 100 µm resolution using appropriate emission and
733 excitation wavelengths, photomultiplier sensitivity and filters for each of the
734 Cy2, Cy3, and Cy5 dyes.
735 Relative protein spot quantification across experimental conditions was
736 performed using DeCyder v7.0 software and multivariate statistical module
737 EDA v7.0 (Extended Data Analysis, GE Healthcare) as follows. First, the
738 Batch Processor module detected spots across the three gel images (two
739 experimental samples and an internal standard) and generates differential in-

gel analysis images with information about spot abundance in each image with values expressed as ratios. After spot detection, the biological variation analysis module utilizes differential in-gel analysis images to match protein spots across all gels, using the internal standard for gel-to-gel matching. Statistical analysis was then carried out to determine protein expression changes. Spot changes with a p-value lower than 0.01 calculated using Student's t-test with the multiple testing assessed using the false discovery rate were considered significant. Multivariate analysis was performed by principal component analysis using the algorithm included in the EDA module of the DeCyder v7.0 software based on spots matched across all gels.

Protein identification was performed at the Proteomics Unit of the Pablo de Olavide University (Seville, Spain) and at the Proteomics service of Parque Científico de Madrid (Madrid, Spain). Spots were excised from the gels manually and transferred to 1.5 mL tubes. Sample digestion and MALDI-MS and MS/MS database searches were done by the Proteomics Units mentioned above.

**Western Blot analyses**

For Western Blot analyses, cells were grown in YEPSL to an $OD_{600}$=0.6-0.8 and were then collected by centrifugation at 4500 rpm for 5 min, washed twice with 20 mM Tris-HCl pH 8.8 and pellets were resuspended in lysis buffer (20 mM Tris-HCl, 0.5 M NaCL, pH 7.4) with protease inhibitor cocktail (cOmplete Tablets, EDTA-free, Roche). Samples lysis was performed with glass beads (Sigma) in a FastPrep®-24 homogeniser (MP Biomedicals), with power set to 6.5 using 6 x 60" pulses at maximum speed with 4 minutes rest between

765 cycles. After cell lysis, tubes were drilled with a needle and put into a new
766 tube and samples were recovered by centrifugation at 4000 rpm for 1 min.
767 Subsequently, samples were centrifuged at 14000 rpm for 30 min at 4ºC and
768 the supernatant was collected. Protein concentration was measured using the
769 RC DC Protein Assay kit (Bio-Rad). 60 µg of protein extract for each strain
770 analyzed was loaded into a 10% TGX Stain-Free™ FastCast™ Acrylamide
771 gel (Bio-Rad). Separated proteins were transferred onto a nitrocellulose
772 membrane using the Trans-Blot® Turbo™ transfer system (Bio-Rad). The
773 membrane was incubated with mouse polyclonal anti-GFP antibody (Roche)
774 (1:1000). As secondary antibody, anti-mouse IgG-horseradish peroxidase
775 conjugated antibody (1:5000; Sigma Aldrich) was used. Immunoreactive
776 bands were developed by SuperSignal™ West Femto Maximum Sensitivity
777 substrate (ThermoFisher Scientific). Image gel and membrane acquisition
778 was carried out with ChemiDoc XRS (Bio-Rad).
779

780 **Microscopy**

781 To corroborate ER Pdi1 localization, experimental SG200*pdi1:gfp* and ER
782 localization control SG200*cal*$^{s}$*:mrfp:HDEL* cells (77) were visualized using a
783 spinning-disk confocal microscope (IX-81, Olympus; CoolSNAP HQ2 camera,
784 Plan Apochromat 100×, 1.4 NA objective, Roper Scientific).
785 For DNA content visualization, cells were stained with DAPI and observed by
786 Differential Interference Contrast (DIC) and fluorescence microscopy using a
787 DeltaVision microscopy system comprising an Olympus IX71 microscope and
788 CoolSnap HQ camera.

For *in planta* quantification of filament and appressoria formation in co-infection experiments with *U. maydis* GFP and RFP labeled strains, 20 dpi leaf samples were stained with calcofluor white (Sigma-Aldrich) to visualize fungal material and then checked for GFP or RFP fluorescence.

To analyze the *U. maydis* progression inside the maize plant, leaf samples from 3 and 5 dpi infected plants were distained with ethanol, treated 4h at 60 ºC with 10% KOH, washed in phosphate buffer and then stained with propidium iodide (PI) to visualize plant tissues in red and wheat germ agglutinin (WGA)/AF488 to visualize the fungus in green. Samples were examined using a Leica SPE (DM2500) confocal microscope. Image processing was carried out using Adobe Photoshop CS5 and ImageJ.

## References

1. Helenius A, Aebi M. Roles of N-Linked Glycans in the Endoplasmic Reticulum. Annu Rev Biochem. 2004 Jun 9;73(1):1019–49.
2. Corfield AP, Berry M. Glycan variation and evolution in the eukaryotes. Trends Biochem Sci. 2015 Jul;40(7):351–9.
3. Freeze HH, Eklund EA, Ng BG, Patterson MC. Neurological Aspects of Human Glycosylation Disorders. Annu Rev Neurosci. 2015 Jul 8;38(1):105–25.
4. Fernandez-Alvarez A, Elias-Villalobos A, Ibeas JI. The O-mannosyltransferase PMT4 is essential for normal appressorium formation and penetration in Ustilago maydis. Plant Cell. 2009;21(10):3397–412.

814 5. Fernandez-Alvarez A, Elias-Villalobos A, Jimenez-Martin A, Marin-
815 Menguiano M, Ibeas JI. Endoplasmic reticulum glucosidases and
816 protein quality control factors cooperate to establish biotrophy in
817 Ustilago maydis. Plant Cell. 2013;25(11):4676–90.
818 6. Olson GM, Fox DS, Wang P, Alspaugh JA, Buchanan KL. Role of
819 protein O-mannosyltransferase Pmt4 in the morphogenesis and
820 virulence of Cryptococcus neoformans. Eukaryot Cell. 2007
821 Feb;6(2):222–34.
822 7. Rouabhia M, Schaller M, Corbucci C, Vecchiarelli A, Prill SK-H,
823 Giasson L, et al. Virulence of the fungal pathogen Candida albicans
824 requires the five isoforms of protein mannosyltransferases. Infect
825 Immun. 2005 Aug 1;73(8):4571–80.
826 8. Schirawski J, Bohnert HU, Steinberg G, Snetselaar K, Adamikowa L,
827 Kahmann R. Endoplasmic Reticulum Glucosidase II Is Required for
828 Pathogenicity of Ustilago maydis. Plant Cell. 2005 Dec 1;17(12):3532–
829 43.
830 9. Schwarz F, Aebi M. Mechanisms and principles of N-linked protein
831 glycosylation. Curr Opin Struct Biol. 2011 Oct;21(5):576–82.
832 10. Breitling J, Aebi M. N-linked protein glycosylation in the endoplasmic
833 reticulum. Cold Spring Harb Perspect Biol. 2013 Aug 1;5(8):a013359.
834 11. Loibl M, Strahl S. Protein O-mannosylation: What we have learned from
835 baker's yeast. Biochim Biophys Acta - Mol Cell Res. 2013
836 Nov;1833(11):2438–46.
837 12. Fabre E, Hurtaux T, Fradin C. Mannosylation of fungal glycoconjugates
838 in the Golgi apparatus. Curr Opin Microbiol. 2014 Aug;20:103–10.

839 13. Hall RA, Gow NAR. Mannosylation in Candida albicans: role in cell wall
840 function and immune recognition. Mol Microbiol. 2013 Dec;90(6):1147–
841 61.
842 14. Oka T, Hamaguchi T, Sameshima Y, Goto M, Furukawa K. Molecular
843 characterization of protein O-mannosyltransferase and its involvement
844 in cell-wall synthesis in Aspergillus nidulans. Microbiology. 2004 Jun
845 1;150(6):1973–82.
846 15. Chen X-L, Shi T, Yang J, Shi W, Gao X, Chen D, et al. N-Glycosylation
847 of Effector Proteins by an α-1,3-Mannosyltransferase Is Required for
848 the Rice Blast Fungus to Evade Host Innate Immunity. Plant Cell. 2014
849 Mar;26(3):1360–76.
850 16. Fernandez-Alvarez A, Marin-Menguiano M, Lanver D, Jimenez-Martin A,
851 Elias-Villalobos A, Perez-Pulido AJ, et al. Identification of O-
852 mannosylated virulence factors in Ustilago maydis. PLoS Pathog.
853 2012;8(3):e1002563.
854 17. Kamper J, Reichmann M, Romeis T, Bolker M, Kahmann R. Multiallelic
855 recognition: nonself-dependent dimerization of the bE and bW
856 homeodomain proteins in Ustilago maydis. Cell. 1995 Apr 7;81(1):73–
857 83.
858 18. Mendoza-Mendoza A, Berndt P, Djamei A, Weise C, Linne U, Marahiel
859 M, et al. Physical-chemical plant-derived signals induce differentiation in
860 Ustilago maydis. Mol Microbiol. 2009;71(4):895–911.
861 19. Kamper J, Kahmann R, Bolker M, Ma LJ, Brefort T, Saville BJ, et al.
862 Insights from the genome of the biotrophic fungal plant pathogen
863 Ustilago maydis. Nature. 2006;444(7115):97–101.

20. Vollmeister E, Schipper K, Baumann S, Haag C, Pohlmann T, Stock J, et al. Fungal development of the plant pathogen Ustilago maydis. FEMS Microbiol Rev. 2012 Jan 1;36(1):59–77.

21. Matei A, Doehlemann G. Cell biology of corn smut disease - Ustilago maydis as a model for biotrophic interactions. Curr Opin Microbiol. 2016;34:60–6.

22. Lanver D, Tollot M, Schweizer G, Lo Presti L, Reissmann S, Ma L-S, et al. Ustilago maydis effectors and their impact on virulence. Nat Rev Microbiol. 2017 May 8;15(7):409–21.

23. Redkar A, Matei A, Doehlemann G. Insights into Host Cell Modulation and Induction of New Cells by the Corn Smut Ustilago maydis. Front Plant Sci. 2017;8:899.

24. Bottin A, Kamper J, Kahmann R. Isolation of a carbon source-regulated gene from Ustilago maydis. Mol Gen Genet. 1996 Dec 13;253(3):342–52.

25. Flor-Parra I, Vranes M, Kamper J, Perez-Martin J. Biz1, a zinc finger protein required for plant invasion by Ustilago maydis, regulates the levels of a mitotic cyclin. Plant Cell. 2006;18(9):2369–87.

26. Djamei A, Schipper K, Rabe F, Ghosh A, Vincon V, Kahnt J, et al. Metabolic priming by a secreted fungal effector. Nature. 2011;478(7369):395–8.

27. Soberanes-Gutierrez C V, Juarez-Montiel M, Olguin-Rodriguez O, Hernandez-Rodriguez C, Ruiz-Herrera J, Villa-Tanaca L. The pep4 gene encoding proteinase A is involved in dimorphism and pathogenesis of Ustilago maydis. Mol Plant Pathol. 2015

Oct;16(8):837–46.

28. Lanver D, Berndt P, Tollot M, Naik V, Vranes M, Warmann T, et al. Plant Surface Cues Prime Ustilago maydis for Biotrophic Development. PLoS Pathog. 2014 Jul 17;10(7):e1004272.

29. Bolker M, Bohnert HU, Braun KH, Gorl J, Kahmann R. Tagging pathogenicity genes in Ustilago maydis by restriction enzyme-mediated integration (REMI). Mol Gen Genet. 1995 Sep;248(5):547–52.

30. Banuett F, Herskowitz I. Different a alleles of Ustilago maydis are necessary for maintenance of filamentous growth but not for meiosis. Proc Natl Acad Sci U S A. 1989;86(15):5878–82.

31. Ali Khan H, Mutus B. Protein disulfide isomerase a multifunctional protein with multiple physiological roles. Front Chem. 2014;2:70.

32. Wilkinson B, Gilbert HF. Protein disulfide isomerase. Biochim Biophys Acta - Proteins Proteomics. 2004;1699(1–2):35–44.

33. Breitenbach M, Weber M, Rinnerthaler M, Karl T, Breitenbach-Koller L. Oxidative stress in fungi: its function in signal transduction, interaction with plant hosts, and lignocellulose degradation. Biomolecules. 2015;5(2):318–42.

34. Banerjee S, Vishwanath P, Cui J, Kelleher DJ, Gilmore R, Robbins PW, et al. The evolution of N-glycan-dependent endoplasmic reticulum quality control factors for glycoprotein folding and degradation. Proc Natl Acad Sci. 2007 Jul 10;104(28):11676–81.

35. Lanver D, Muller AN, Happel P, Schweizer G, Haas FB, Franitza M, et al. The biotrophic development of Ustilago maydis studied by RNAseq analysis. Plant Cell. 2018;30(February):tpc.00764.2017.

914 36. Brefort T, Tanaka S, Neidig N, Doehlemann G, Vincon V, Kahmann R.
915 Characterization of the largest effector gene cluster of Ustilago maydis.
916 PLoS Pathog. 2014;10(7):e1003866.
917 37. Harries E, Gandia M, Carmona L, Marcos JF. The Penicillium digitatum
918 protein O-mannosyltransferase Pmt2 is required for cell wall integrity,
919 conidiogenesis, virulence and sensitivity to the antifungal peptide
920 PAF26. Mol Plant Pathol. 2015 Sep;16(7):748–61.
921 38. Guo M, Tan L, Nie X, Zhu X, Pan Y, Gao Z. The Pmt2p-Mediated
922 Protein O-Mannosylation Is Required for Morphogenesis, Adhesive
923 Properties, Cell Wall Integrity and Full Virulence of Magnaporthe oryzae.
924 Front Microbiol. 2016 May 2;7:630.
925 39. Gonzalez M, Brito N, Frias M, Gonzalez C. Botrytis cinerea Protein O-
926 Mannosyltransferases Play Critical Roles in Morphogenesis, Growth,
927 and Virulence. Yu J-H, editor. PLoS One. 2013 Jun 6;8(6):e65924.
928 40. Wagener J, Weindl G, de Groot PWJ, de Boer AD, Kaesler S, Thavaraj
929 S, et al. Glycosylation of Candida albicans cell wall proteins is critical for
930 induction of innate immune responses and apoptosis of epithelial cells.
931 Lenz LL, editor. PLoS One. 2012 Nov 30;7(11):e50518.
932 41. Willger SD, Ernst JF, Alspaugh JA, Lengeler KB. Characterization of the
933 PMT gene family in Cryptococcus neoformans. Lin X, editor. PLoS One.
934 2009 Jul 27;4(7):e6321.
935 42. Leach MD, Brown AJP. Posttranslational Modifications of Proteins in
936 the Pathobiology of Medically Relevant Fungi. Eukaryot Cell. 2012
937 Feb;11(2):98–108.
938 43. Uhse S, Djamei A. Effectors of plant-colonizing fungi and beyond. Zipfel

C, editor. PLOS Pathog. 2018 Jun 7;14(6):e1006992.

44. Xie X, Lipke PN. On the evolution of fungal and yeast cell walls. Yeast. 2010 Jun 2;27(8):479–88.

45. Kruszewska JS, Perlińska-Lenart U, Górka-Nieć W, Orłowski J, Zembek P, Palamarczyk G. Alterations in protein secretion caused by metabolic engineering of glycosylation pathways in fungi. Acta Biochim Pol. 2008;55(3):447–56.

46. Nielsen H. Predicting Secretory Proteins with SignalP. In: Methods in molecular biology (Clifton, NJ). 2017. p. 59–73.

47. Sperschneider J, Dodds PN, Singh KB, Taylor JM. ApoplastP : prediction of effectors and plant proteins in the apoplast using machine learning. New Phytol. 2018 Mar;217(4):1764–78.

48. Sperschneider J, Gardiner DM, Dodds PN, Tini F, Covarelli L, Singh KB, et al. Effector P: predicting fungal effector proteins from secretomes using machine learning. New Phytol. 2016 Apr;210(2):743–61.

49. Burggraaf A-M, Punt PJ, Ram AFJ. The unconventional secretion of PepN is independent of a functional autophagy machinery in the filamentous fungus Aspergillus niger. FEMS Microbiol Lett. 2016 Aug;363(15).

50. Koepke J, Kaffarnik F, Haag C, Zarnack K, Luscombe NM, Konig J, et al. The RNA-Binding Protein Rrm4 is Essential for Efficient Secretion of Endochitinase Cts1. Mol Cell Proteomics. 2011 Dec;10(12):M111.011213.

51. Stock J, Sarkari P, Kreibich S, Brefort T, Feldbrugge M, Schipper K. Applying unconventional secretion of the endochitinase Cts1 to export

964 heterologous proteins in Ustilago maydis. J Biotechnol. 2012 Oct
965 15;161(2):80–91.
966 52. Aschenbroich J, Hussnaetter KP, Stoffels P, Langner T, Zander S,
967 Sandrock B, et al. The germinal centre kinase Don3 is crucial for
968 unconventional secretion of chitinase Cts1 in Ustilago maydis. Biochim
969 Biophys Acta - Proteins Proteomics. 2018;
970 53. Paper JM, Scott-Craig JS, Adhikari ND, Cuomo CA, Walton JD.
971 Comparative proteomics of extracellular proteins in vitro and in planta
972 from the pathogenic fungus Fusarium graminearum. Proteomics. 2007
973 Sep;7(17):3171–83.
974 54. Lanver D, Mendoza-Mendoza A, Brachmann A, Kahmann R. Sho1 and
975 Msb2-related proteins regulate appressorium development in the smut
976 fungus Ustilago maydis. Plant Cell. 2010;22(6):2085–101.
977 55. Tollot M, Assmann D, Becker C, Altmuller J, Dutheil JY, Wegner C-E, et
978 al. The WOPR Protein Ros1 Is a Master Regulator of Sporogenesis and
979 Late Effector Gene Expression in the Maize Pathogen Ustilago maydis.
980 Wang Y, editor. PLoS Pathog. 2016 Jun 22;12(6):e1005697.
981 56. Wahl R, Zahiri A, Kamper J. The Ustilago maydis b mating type locus
982 controls hyphal proliferation and expression of secreted virulence
983 factors in planta. Mol Microbiol. 2010 Jan;75(1):208–20.
984 57. Skibbe DS, Doehlemann G, Fernandes J, Walbot V. Maize tumors
985 caused by Ustilago maydis require organ-specific genes in host and
986 pathogen. Science (80- ). 2010;328(5974):89–92.
987 58. Zhou X, Liu W, Wang C, Xu Q, Wang Y, Ding S, et al. A MADS-box
988 transcription factor MoMcm1 is required for male fertility, microconidium

production and virulence in Magnaporthe oryzae. Mol Microbiol. 2011 Apr;80(1):33–53.

59. Pan Y, Pan R, Tan L, Zhang Z, Guo M. Pleiotropic roles of O-mannosyltransferase MoPmt4 in development and pathogenicity of Magnaporthe oryzae. Curr Genet. 2018 Jun 26;

60. Li M, Liu X, Liu Z, Sun Y, Liu M, Wang X, et al. Glycoside Hydrolase MoGls2 Controls Asexual/Sexual Development, Cell Wall Integrity and Infectious Growth in the Rice Blast Fungus. Wang Z, editor. PLoS One. 2016 Sep 8;11(9):e0162243.

61. Fernandez-Alvarez A, Elias-Villalobos A, Ibeas JI. The requirement for protein O-mannosylation for Ustilago maydis virulence seems to be linked to intrinsic aspects of the infection process rather than an altered plant response. Plant Signal Behav. 2010;5(4):412–4.

62. Win J, Chaparro-Garcia A, Belhaj K, Saunders DGO, Yoshida K, Dong S, et al. Effector Biology of Plant-Associated Organisms: Concepts and Perspectives. Cold Spring Harb Symp Quant Biol. 2012 Jan 1;77(0):235–47.

63. Seitner D, Uhse S, Gallei M, Djamei A. The core effector Cce1 is required for early infection of maize by Ustilago maydis. Mol Plant Pathol. 2018;19(10):2277–87.

64. Trombetta ES, Parodi AJ. Quality Control and Protein Folding in the Secretory Pathway. Annu Rev Cell Dev Biol. 2003 Nov 28;19(1):649–76.

65. Moremen KW, Molinari M. N-linked glycan recognition and processing: the molecular basis of endoplasmic reticulum quality control. Curr Opin Struct Biol. 2006 Oct;16(5):592–9.

66. Doehlemann G, van der Linde K, Assmann D, Schwammbach D, Hof A, Mohanty A, et al. Pep1, a secreted effector protein of Ustilago maydis, is required for successful invasion of plant cells. PLoS Pathog. 2009;5(2):e1000290.

67. Hemetsberger C, Herrberger C, Zechmann B, Hillmer M, Doehlemann G. The Ustilago maydis effector Pep1 suppresses plant immunity by inhibition of host peroxidase activity. PLoS Pathog. 2012;8(5):e1002684.

68. Mueller AN, Ziemann S, Treitschke S, Assmann D, Doehlemann G. Compatibility in the Ustilago maydis-maize interaction requires inhibition of host cysteine proteases by the fungal effector Pit2. PLoS Pathog. 2013;9(2):e1003177.

69. Redkar A, Hoser R, Schilling L, Zechmann B, Krzymowska M, Walbot V, et al. A Secreted Effector Protein of Ustilago maydis Guides Maize Leaf Cells to Form Tumors. Plant Cell. 2015;27(4):1332–51.

70. Sambrook J, Frisch E, Maniatis T. Molecular cloning: a laboratory manual, 2nd ed. 2nd ed. Cold Spring Harbor, NY: Cold Spring Harbor Laboratory Press; 1989.

71. Gillissen B, Bergemann J, Sandmann C, Schroeer B, Bolker M, Kahmann R. A two-component regulatory system for self/non-self recognition in Ustilago maydis. Cell. 1992;68(4):647–57.

72. Schulz B, Banuett F, Dahl M, Schlesinger R, Schafer W, Martin T, et al. The b alleles of U. maydis, whose combinations program pathogenic development, code for polypeptides containing a homeodomain-related motif. Cell. 1990;60(2):295–306.

73. Brachmann A, Konig J, Julius C, Feldbrugge M. A reverse genetic

approach for generating gene replacement mutants in Ustilago maydis. Mol Genet Genomics. 2004;272(2):216–26.

74. Fuchs U, Hause G, Schuchardt I, Steinberg G. Endocytosis is essential for pathogenic development in the corn smut fungus Ustilago maydis. Plant Cell. 2006 Aug;18(8):2066–81.

75. Wedlich-Soldner R, Bolker M, Kahmann R, Steinberg G. A putative endosomal t-SNARE links exo- and endocytosis in the phytopathogenic fungus Ustilago maydis. Embo J. 2000;19(9):1974–86.

76. Pitarch A, Sanchez M, Nombela C, Gil C. Sequential fractionation and two-dimensional gel analysis unravels the complexity of the dimorphic fungus Candida albicans cell wall proteome. Mol Cell Proteomics. 2002;1(12):967–82.

77. Theisen U, Straube A, Steinberg G. Dynamic rearrangement of nucleoporins during fungal "open" mitosis. Mol Biol Cell. 2008 Mar;19(3):1230–40.

## Supporting information

**S1 Fig. Um10156 is similar to *Saccharomyces cerevisiae* Pdi1.** Alignment of Pdi1 sequence from *S. cerevisiae* and Um10156 from *U. maydis* using T-Coffee Server and BoxShade Server. Thioredoxin domains are indicated by red lines.

**S2 Fig. Loss of *pdi1* has no effect on the non-pathogenic stage.** (A) Growth rate of SG200 and SG200 Δ*pdi1* in liquid rich media YEPSL. (B)

SG200 and Δ*pdi1* cells observed by DIC microscopy don't show any defect in size and morphology.

**S3 Fig. N-glycosylation mutation in Pdi1 does not affect cell wall integrity nor oxidative stress.** ER stress, cell wall integrity and oxidative assays were performed in CM plates supplemented with 2% D-glucose and calcofluor white (CFW) 40 µg/ml, Congo Red 50 µg/ml, Tunicamycin 1 µg/ml, Sorbitol 1M, 2% DMSO, $H_2O_2$ 1.5 mM and NaCl 1M.

**S1 Table. Identified glycoproteins in this study.** List of glycoproteins identified through the tree different extracts indicating in which extract were identified, their apoplastic secretion prediction and their gene deletion phenotypes after maize plant infection.

**S2 Table. List of strains used in this study.**

**S3 Table. List of primers used in this study.**

## Figure captions

**Fig 1. Proteomic approach to identify glycoproteins involved in virulence.** *Biz1* overexpression is used to induce the pathogenic pathway and cytosolic proteins are then collected from wild-type *U. maydis* and from a mutant deficient in either O- or N- glycosylation. O- or N-glycoproteins are purified through a Concanavalin A FPLC column using O- or N-glycoprotein specific eluents. Finally, glycoproteins are tagged with fluorophores and separated by 2D electrophoresis.

**Fig 2. 2D-DIGE expression analysis of Pmt4 and Gls1- dependent cytoplasmic glycoproteins.** Cells growing in inducing conditions develop hyphae (A). Images of DIGE gels containing an internal standard loaded with equal amounts of each sample, showing protein changes between *biz1* and *pmt4*-mutants (B) or *biz1* and *gls1*-mutants (C). Protein expression profile changes between wild-type *biz1*$^{crg}$ vs Δ*pmt4* mutants (D) or Δ*gls1* mutants (E) showed by the DeCyder software analysis. The edge of the indicated protein is displayed in the DIGE gel in pink and in a specific zoom in yellow.

**Fig 3. 2D-DIGE expression analysis of Pmt4 and Gls1- dependent secreted or cell wall glycoproteins.** Images of the DIGE gels containing an internal standard loaded with equal amounts of each samples, showing protein changes between wild-type *biz1*$^{crg}$ and *pmt4*-mutants (secreted glycoproteins in A, left part; cell wall glycoproteins in B, left part) or wild-type *biz1*$^{crg}$ and *gls1*-mutants (A, right part; B right part).

**Fig 4. Infection assay of pathogenic pathway glycoprotein candidates.** Deletions and infections were first carried out in the CL13 strain (A). Deletions showing a statistically significant reduction in virulence were then assayed in SG200 (B) and subsequently in FB1 and FB2 compatible strains (C). Total number of plants infected is indicated above each column. The Mann-Whitney statistical test was performed for each mutant versus the corresponding wild-type strain (ns: not statistically significant; * for p-value < 0.05; ** for p-value < 0.01; *** for p-value < 0.005; **** for p-value < 0.0001). (D) Representative Δ*Um10156* disease symptoms compared to wild-type.

**Fig 5. Pdi1 (Um10156) is a protein disulfide isomerase that localizes to the ER and its deletion results in sensitivity to ER stress inducing treatments.** (A) Schematic representation of ScPdi1 and Um10156 showing signal peptides (SP), thioredoxin domains, WCGHCK active sites, HDEL/HEEL ER localization sites and thioredoxin domain and whole protein identity percentages obtained by BLASTp. (B) Pdi1:GFP co-localizes with the ER marker mRFP:HDEL. (C) ER stress assay was performed on solid CM plates supplemented with 2% D-glucose and 4 mM DTT. (D) ER stress assay performed with liquid media supplemented with 10 mM DTT. Scale bar represents 5 μm.

**Fig 6. Pdi1 is essential for fungal growth within the maize plant.** Mating assay between compatible *U. maydis* strains, FB1 and FB2 Δ*pdi1* strains were tested on PD-charcoal (PD-Ch) plates (A). Maize seedlings were co-infected with SG200 GFP and SG200 Δ*pdi1* RFP strains. After 20h, filament (B) and appressoria (C) formation were measured by scoring for GFP or RFP fluorescence. Total number of plants infected is indicated above each column. Scale bar represents 5 μm. (D) Maize leaves from 3 and 5 dpi plants infected with SG200 and SG200Δ*pdi1* were stained with propidium iodide (red) and *U. maydis* hyphae with WGA-AF-488 (green), and visualized by fluorescence microscopy, showing a decrease in the growth and branching capability of the *pdi1* mutant. Scale bar represents 50 μm. (E) Quantification of fungal biomass in planta at 3 dpi was performed by qPCR, measuring the constitutively-

expressed *ppi1 U. maydis* gene normalized to the constitutively-expressed plant *gapdh* gene, confirming its defective proliferation. T-test statistical analysis was performed (* for p-value < 0.05).

**Fig 7. Pdi1 mRNA and protein expression profiles.** (A) *pdi1* expression levels relative to *ppi1* during maize plant infection calculated by qRT-PCR from RNA isolated from plants infected with FB1 x FB2 at 1, 3, 5 and 9 days post infection and RNA from axenic culture. (B) Pdi1 protein expression profile before and after *biz1* activation obtained by DiGE analysis.

**Fig 8. N-glycosylation of the protein disulfide isomerase Pdi1 ensures *U. maydis* virulence.** (A) Pdi1 has two putative N-glycosylation sites and eight putative O-glycosylation sites. The main amino acids where the glycosylation tree is anchored, serine/threonine in O-glycosylation and asparagine in N-glycosylation, have been replaced by similar amino acids alanine and glutamine for O- and N-glycosylation, respectively. (B) The percentage of symptoms in maize plants infected with the indicated strains at 14 dpi. The total number of infected plants is indicated above each column. Mann-Whitney statistical test was performed (ns: not statistically significant; **** for p-value < 0.0001). Representative disease symptoms are shown above. (C) Quantification of fungal biomass in planta at 5 dpi was performed by qPCR, measuring the constitutively-expressed *ppi1 U. maydis* gene normalized to the constitutively-expressed plant *gapdh* gene. T-test statistical analysis was performed (ns for not statistically significant, * for p-value < 0.05, ** for p-value < 0.01). (D) Western blot showing Pdi1:GFP in SG200 and Pdi1_ΔN-

glycosylation:GFP in SG200 Δ*pdi1*, with the image of the stain-free gel activation as a loading control. (E) Indicated strains were spotted onto CM plates supplemented with 2% D-glucose and 4 mM DTT. The mutation of N-glycosylation sites resulted on high DTT sensitivity.

**Fig 9. 2D-DIGE expression analysis of Gls1- or Pdi1- dependent secreted glycoproteins.** DIGE gel images showing protein changes between wild-type *biz1*$^{crg}$ (tagged with Cy3 – green) and *gls1* (tagged with Cy5 – red) mutants (A) or between wild-type *biz1*$^{crg}$ (tagged with Cy3 – green) and *pdi1* (tagged with Cy5 – red) mutants (B). Several glycoproteins depending on both Gls1 and Pdi1 could be identified. Three such proteins are indicated on the gels by dotted rectangles.

**Fig 10. Model of Pdi1 function during infection.** Pdi1 assists a subset glycoprotein in folding and disulfide bonds formation during effector secretion in the apoplast of maize plant during *U. maydis* infection.

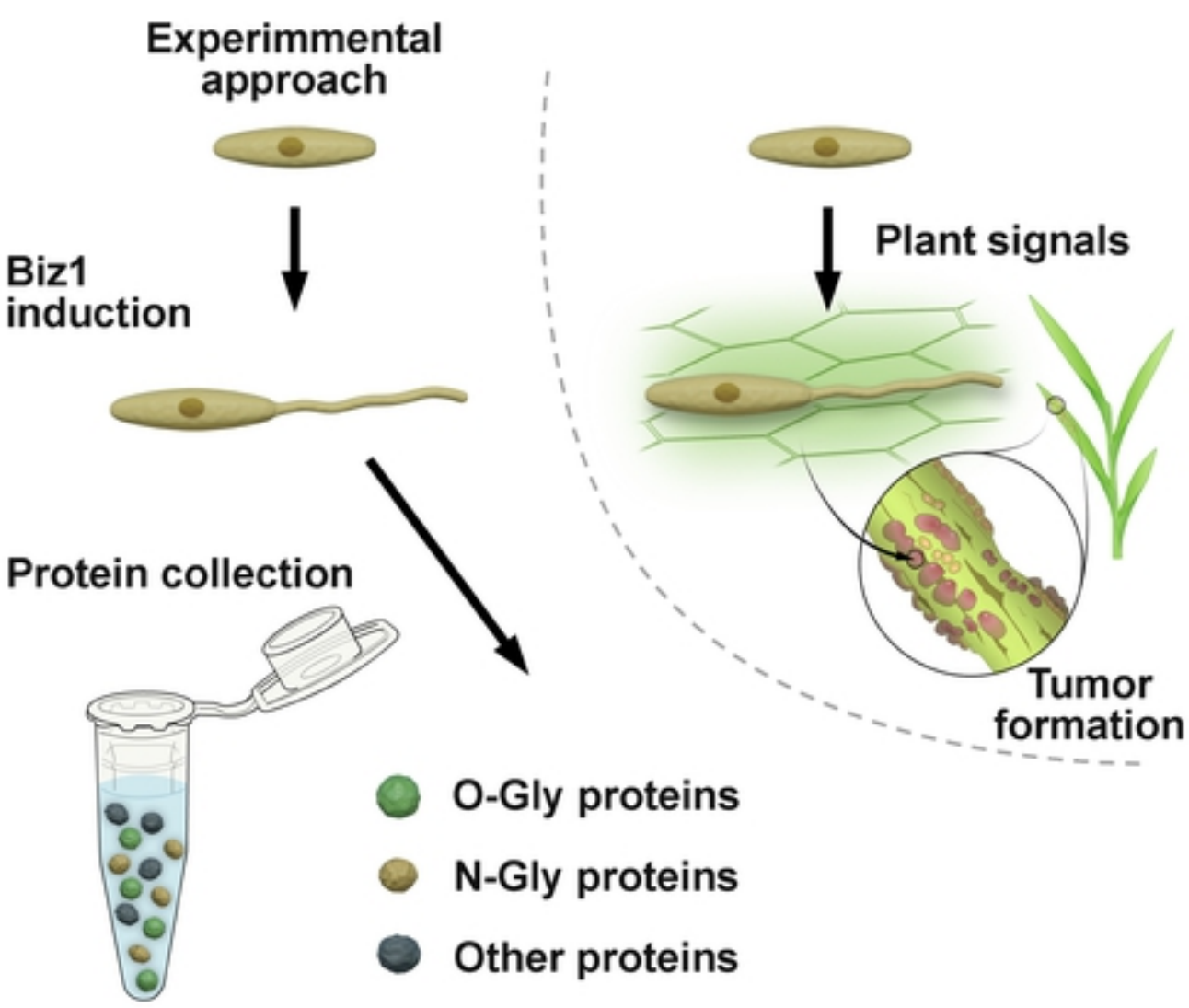




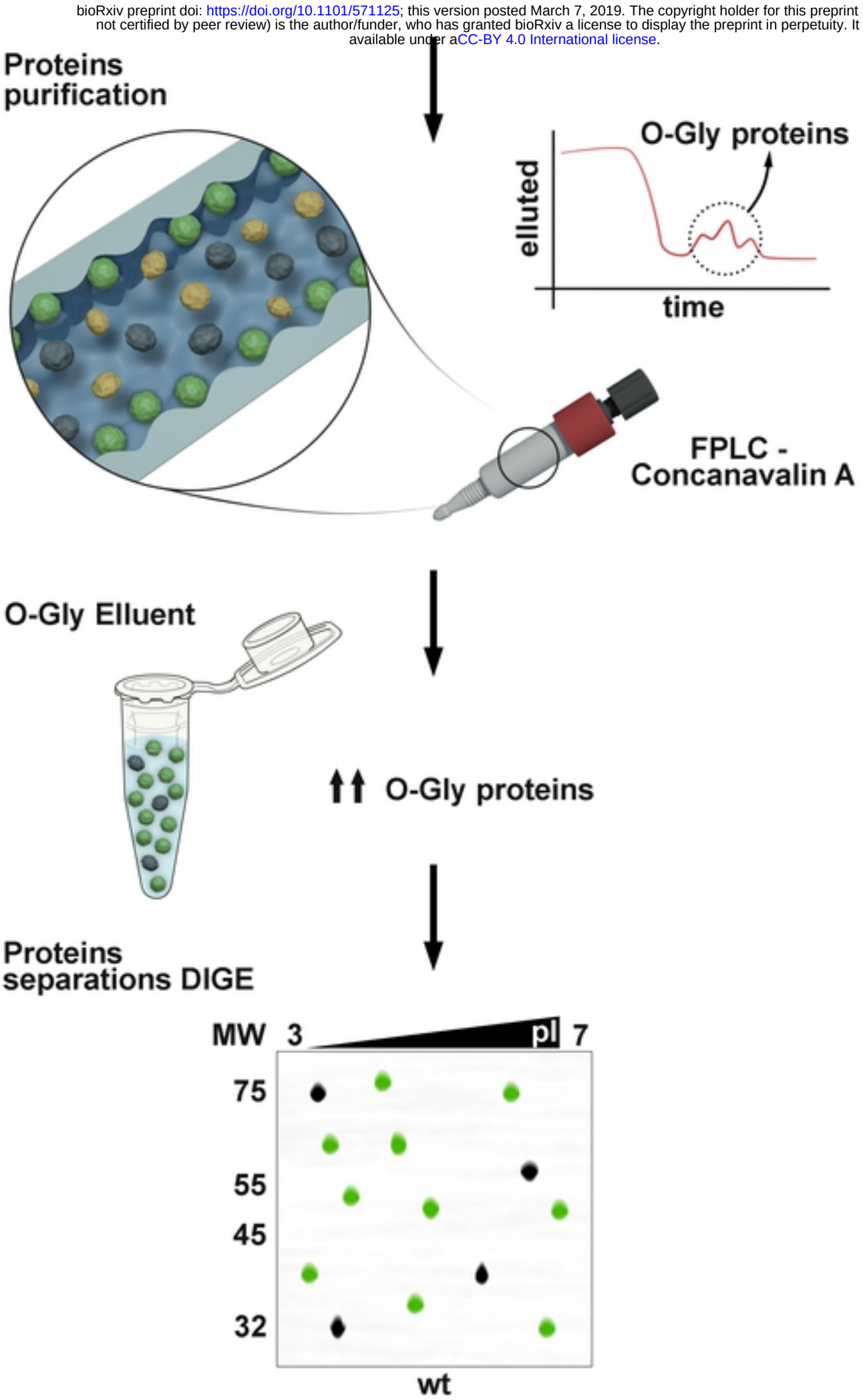


Figure 1

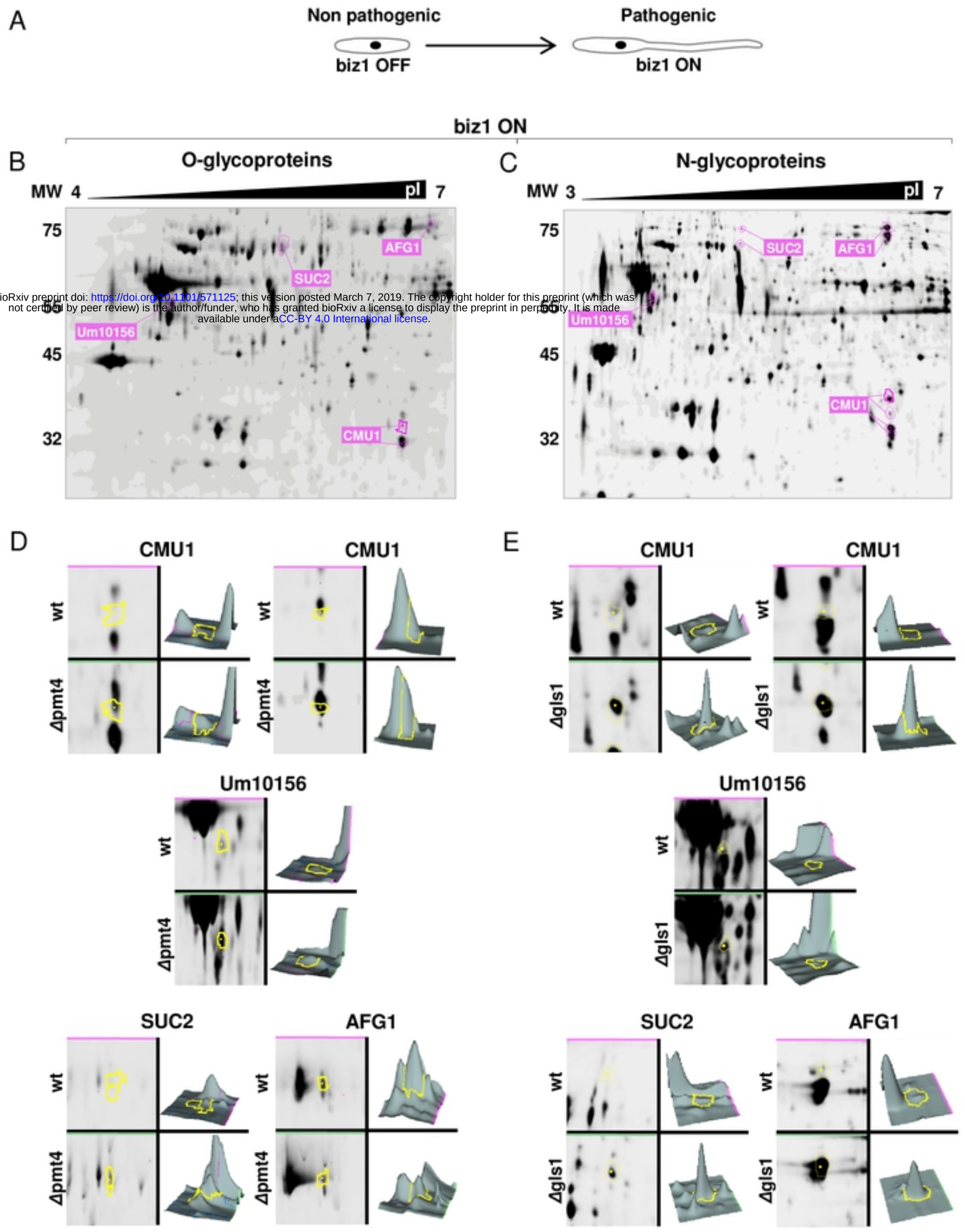


Figure 2

A

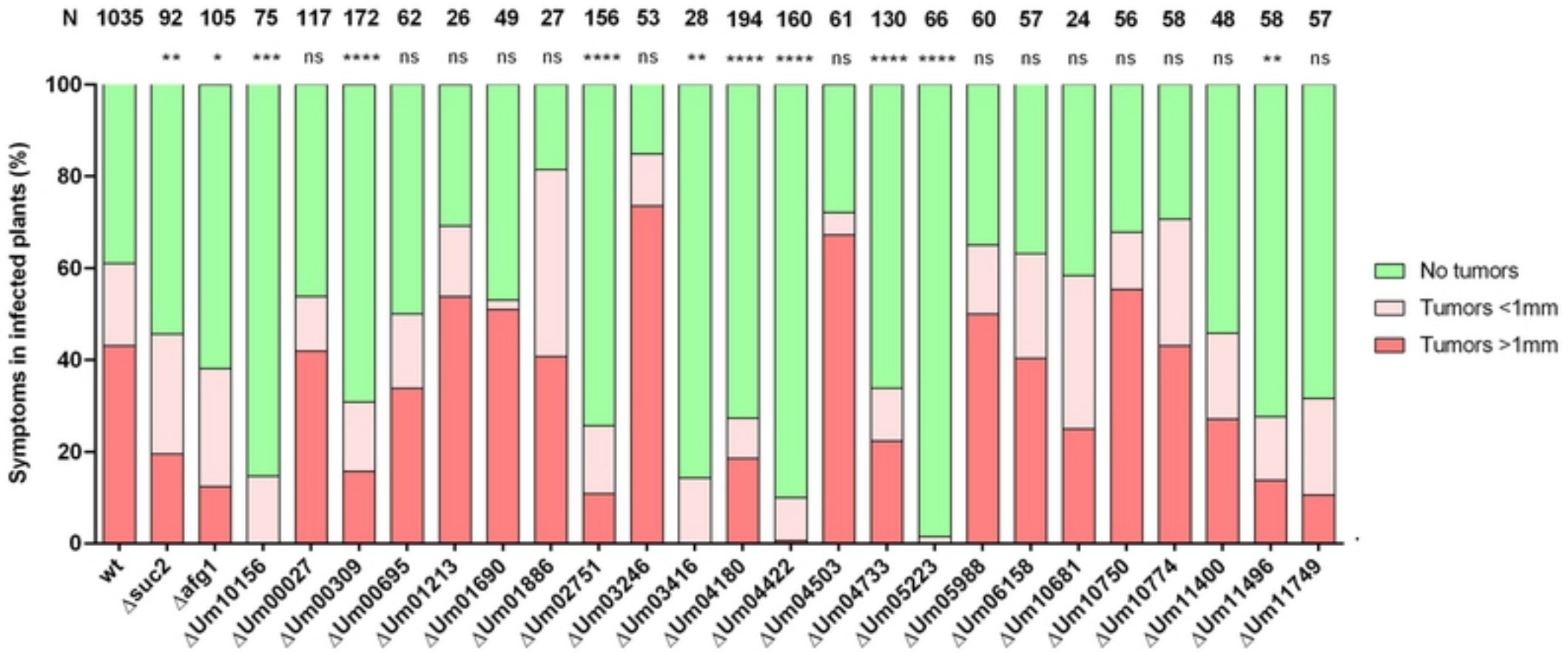




B

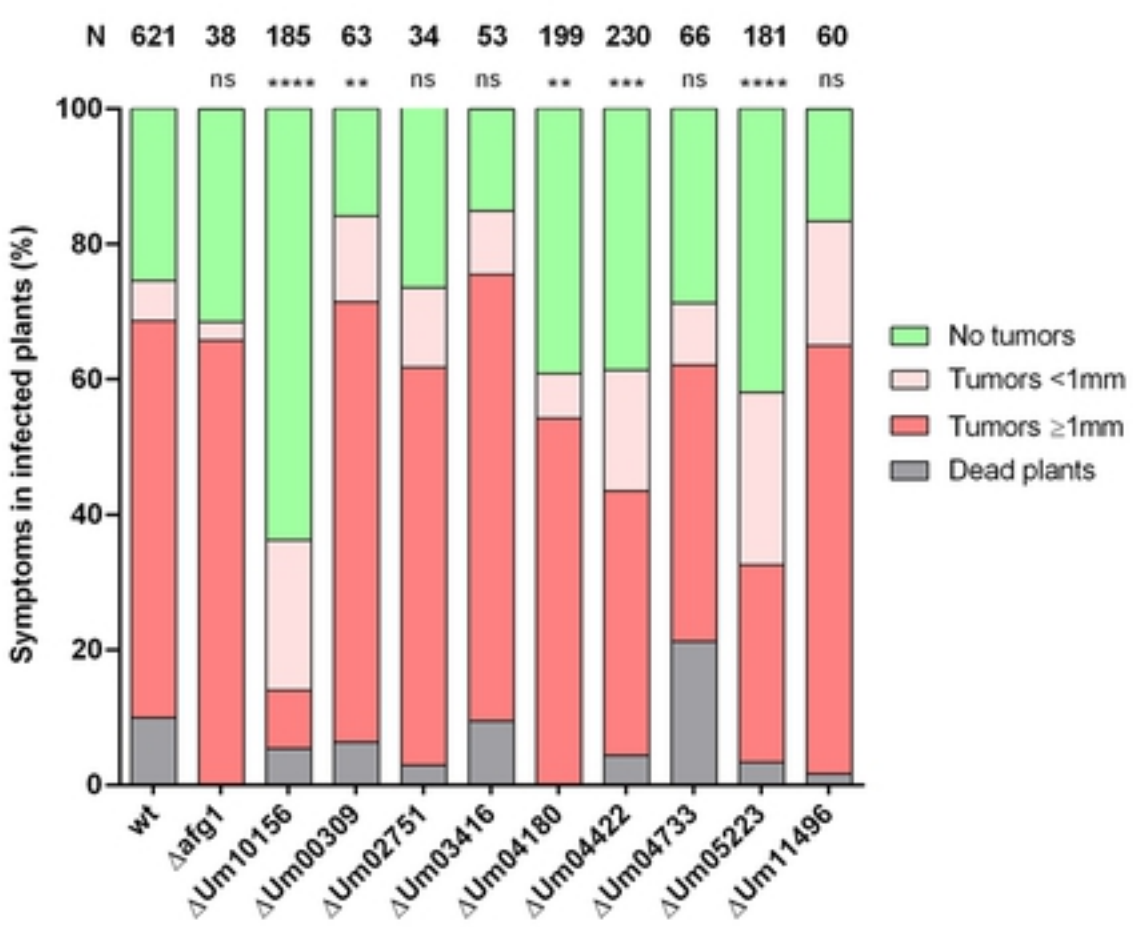


C

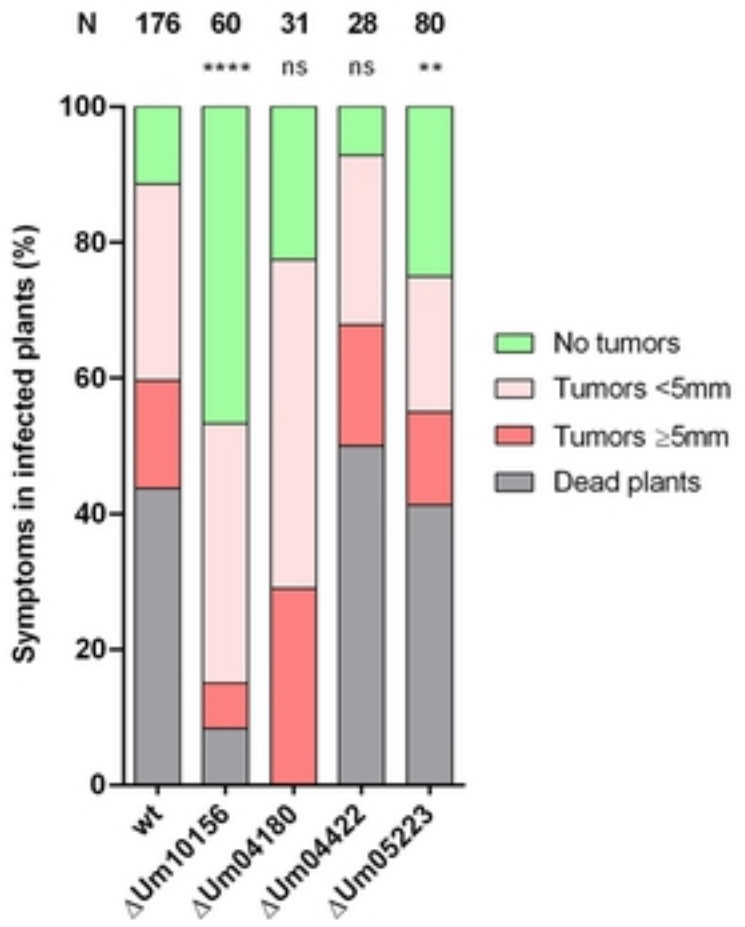


D

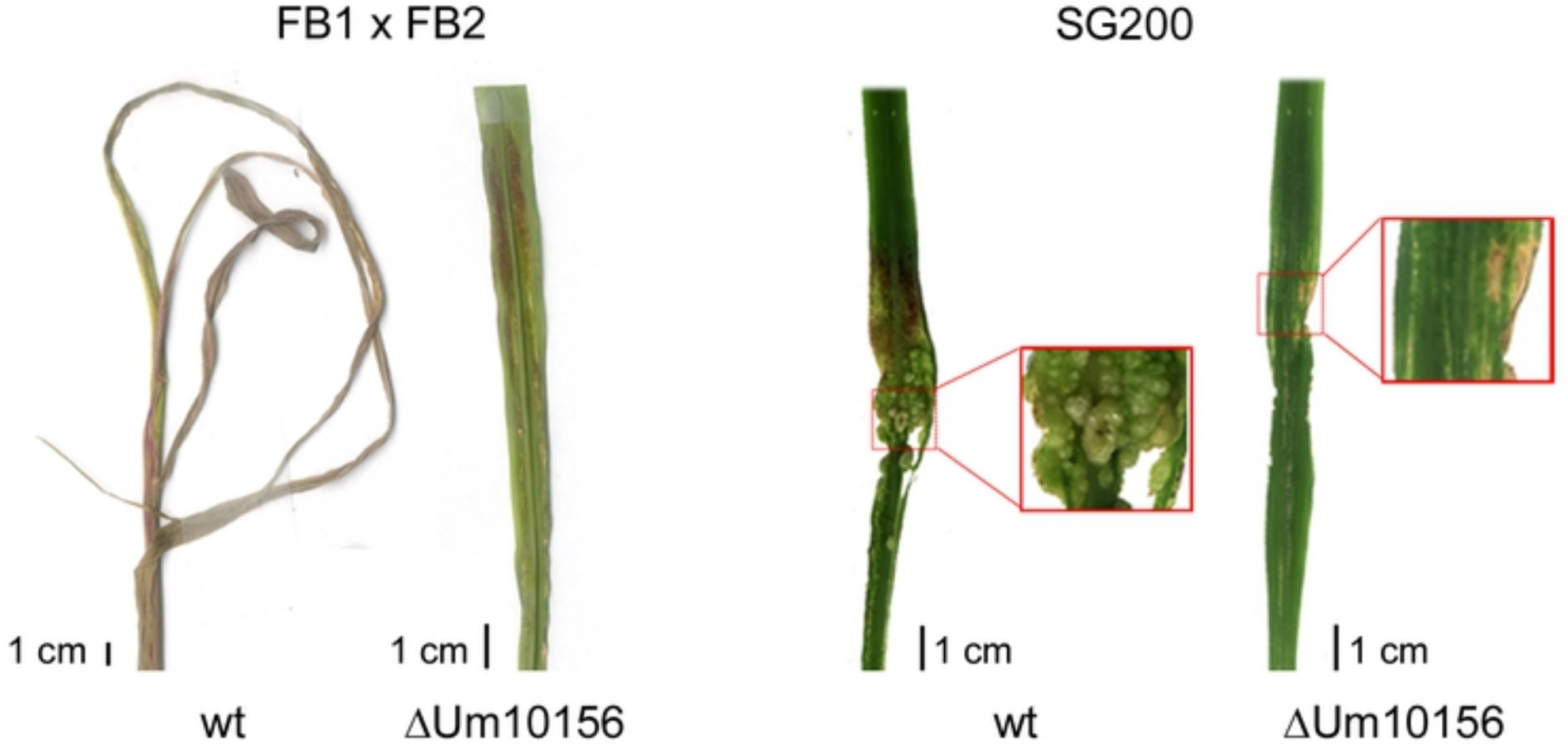


Figure 4

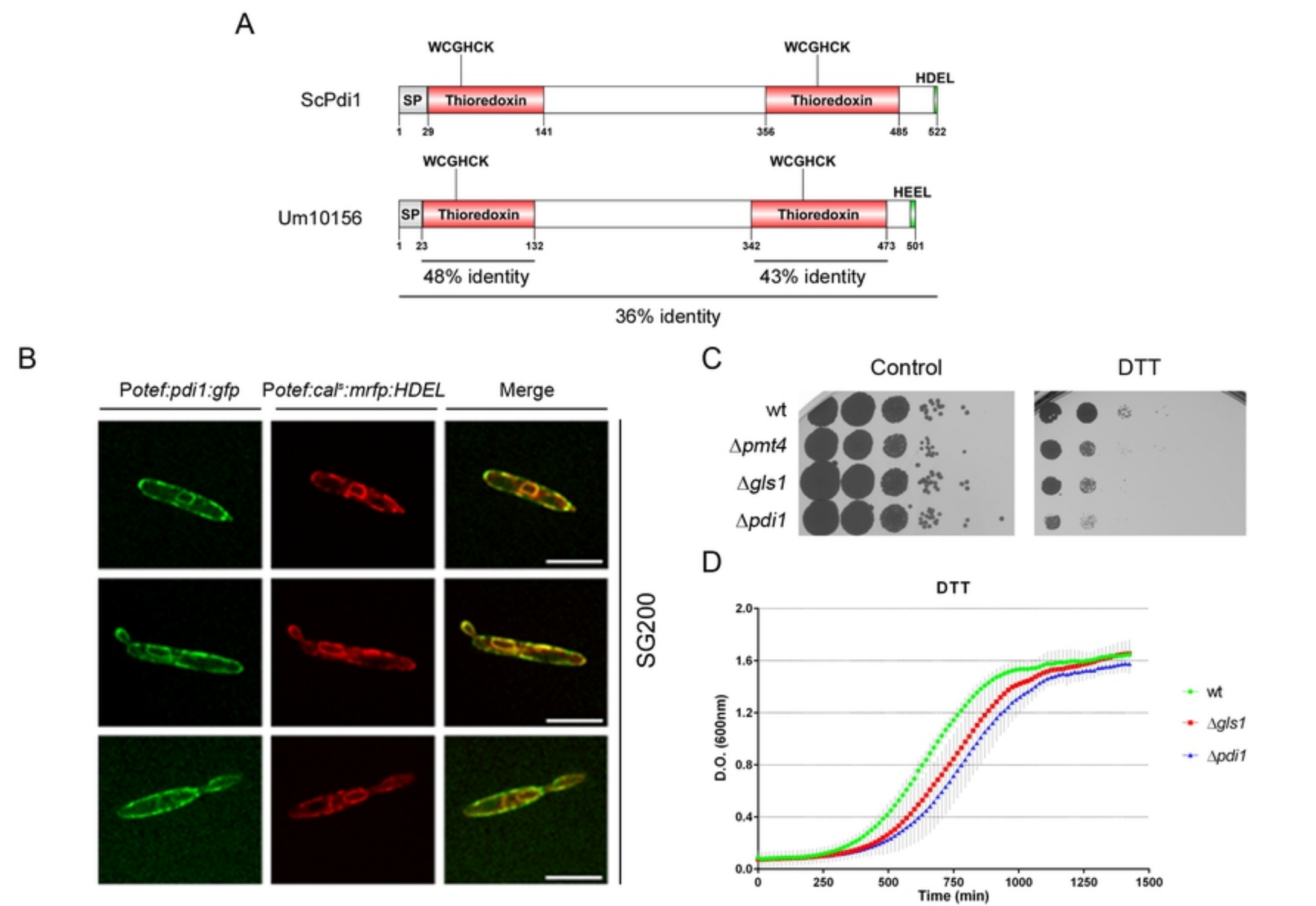
A
WCGHCK
WCGHCK
HDEL
ScPdi1
SP
Thioredoxin
Thioredoxin
1
29
141
356
485
522
WCGHCK
WCGHCK
HEEL
Um10156
SP
Thioredoxin
Thioredoxin
1
23
132
342
473
501
48% identity
43% identity
36% identity
B
Potef:pdi1:gfp
Potef:cal$^s$:mrfp:HDEL
Merge
SG200
C
Control
DTT
wt
Δpmt4
Δgls1
Δpdi1
D
DTT
D.O. (600nm)
Time (min)
wt
Δgls1
Δpdi1

Figure 5

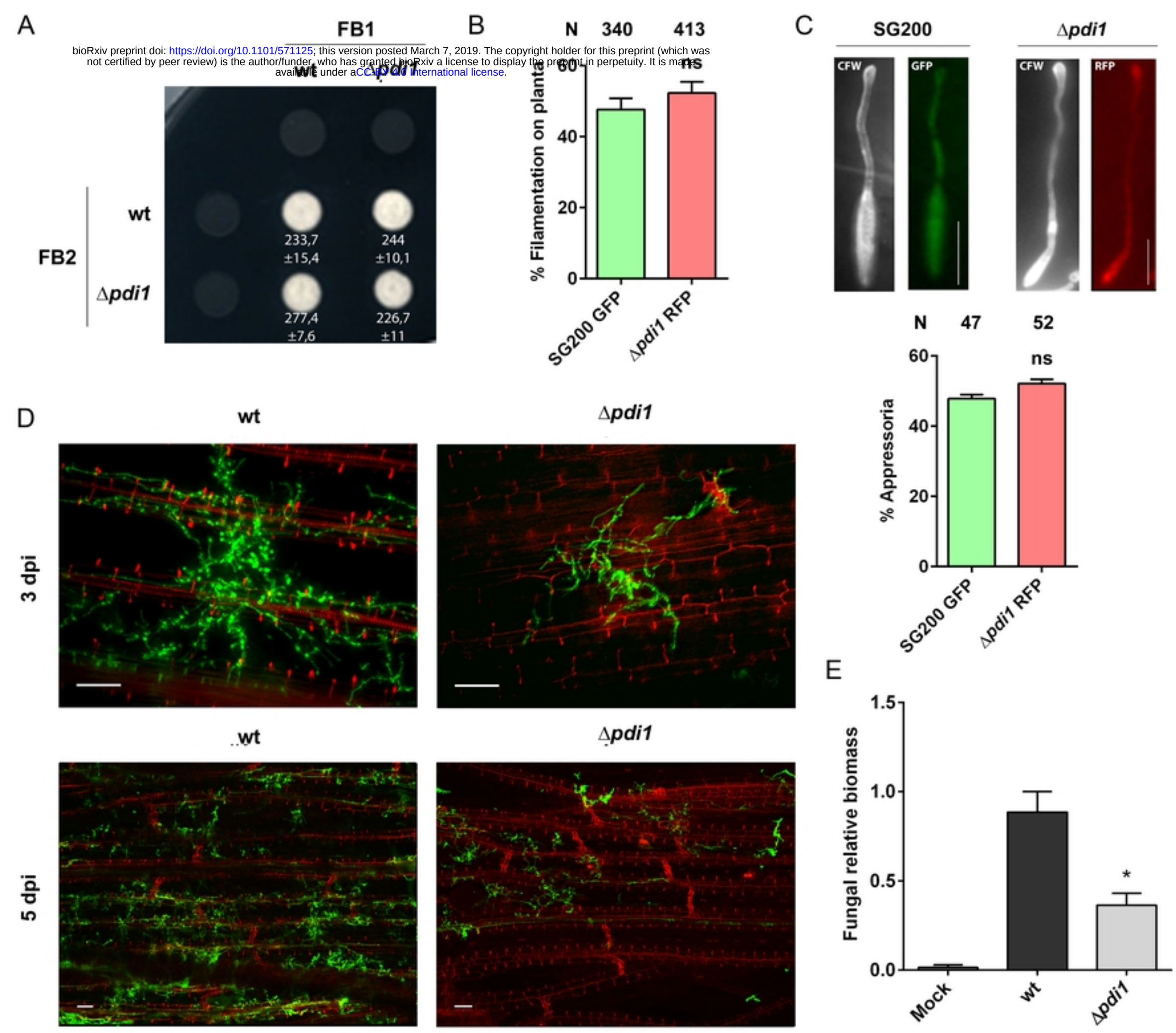


Figure 6

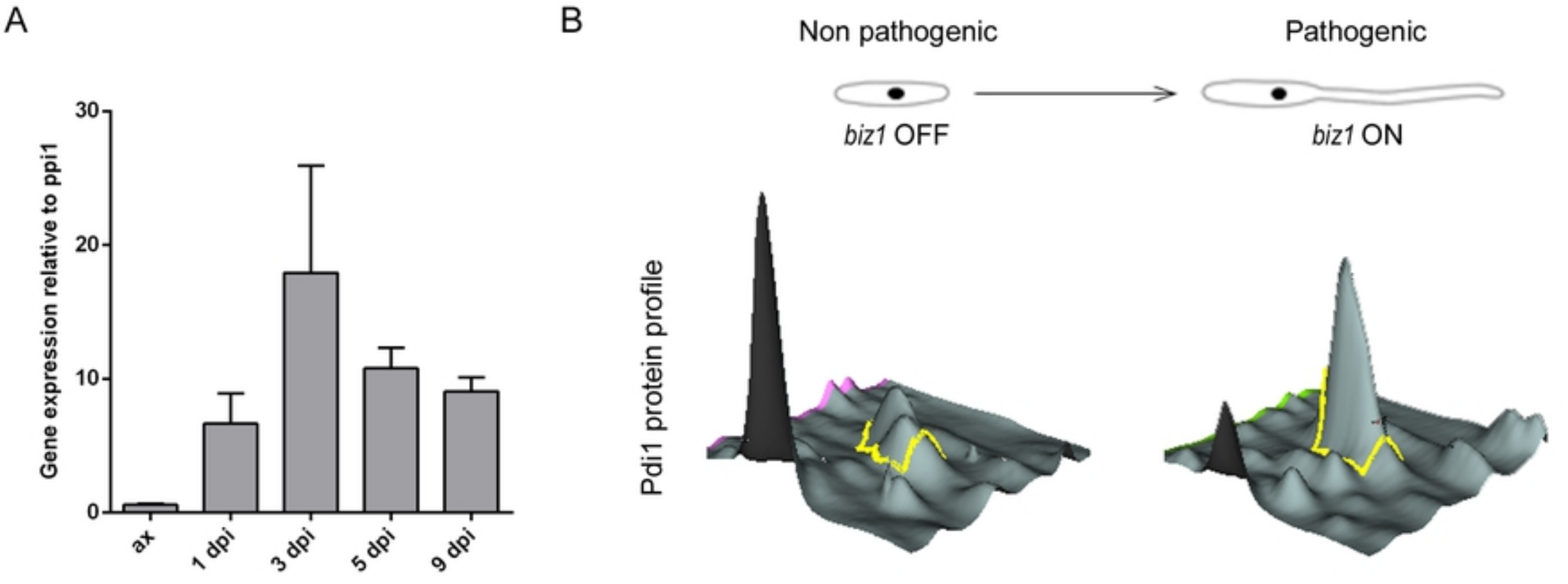
A
Gene expression relative to ppi1
30
20
10
0
ax
1 dpi
3 dpi
5 dpi
9 dpi
B
Non pathogenic
Pathogenic
biz1 OFF
biz1 ON
Pdi1 protein profile

Figure 7

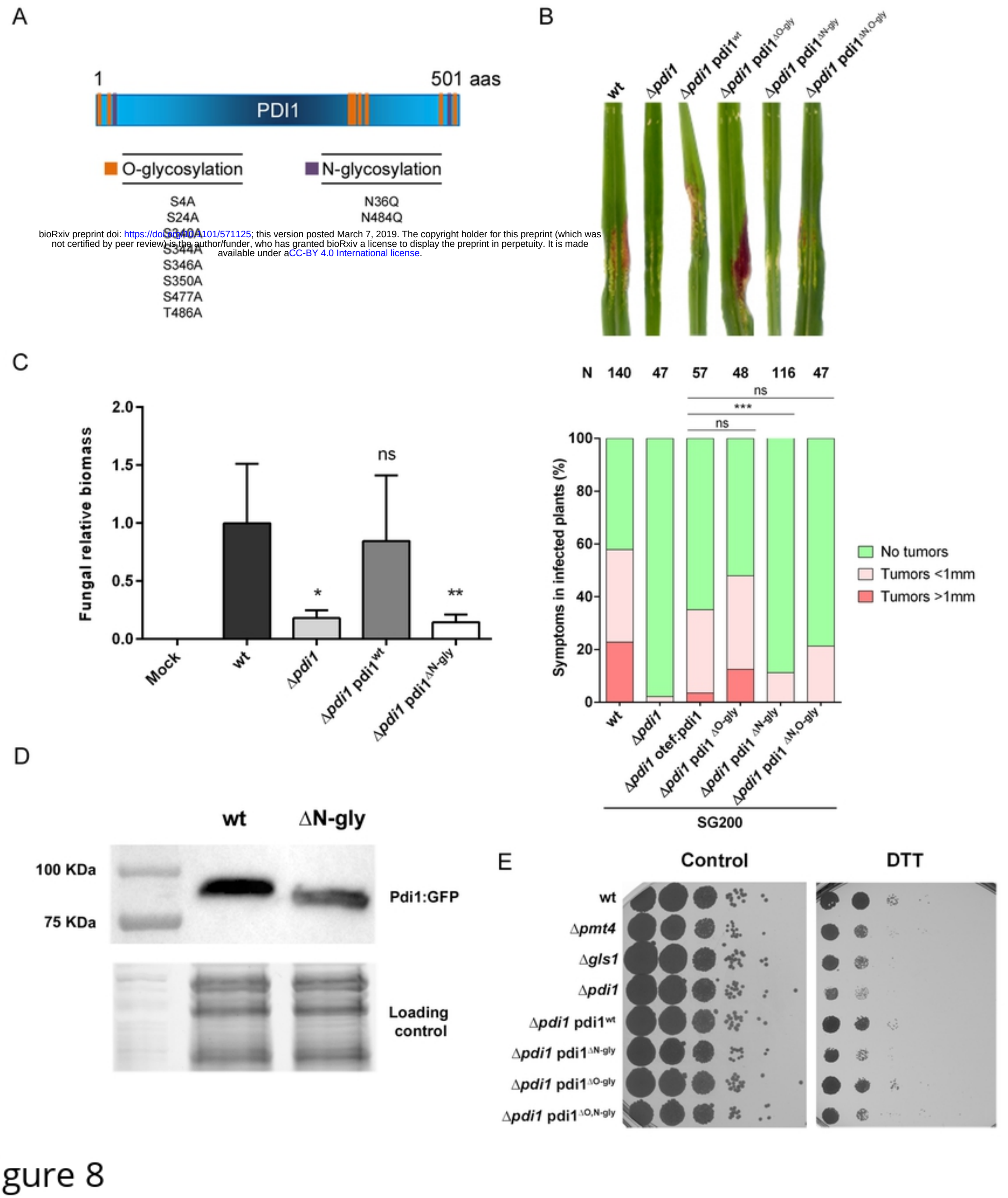


Figure 8

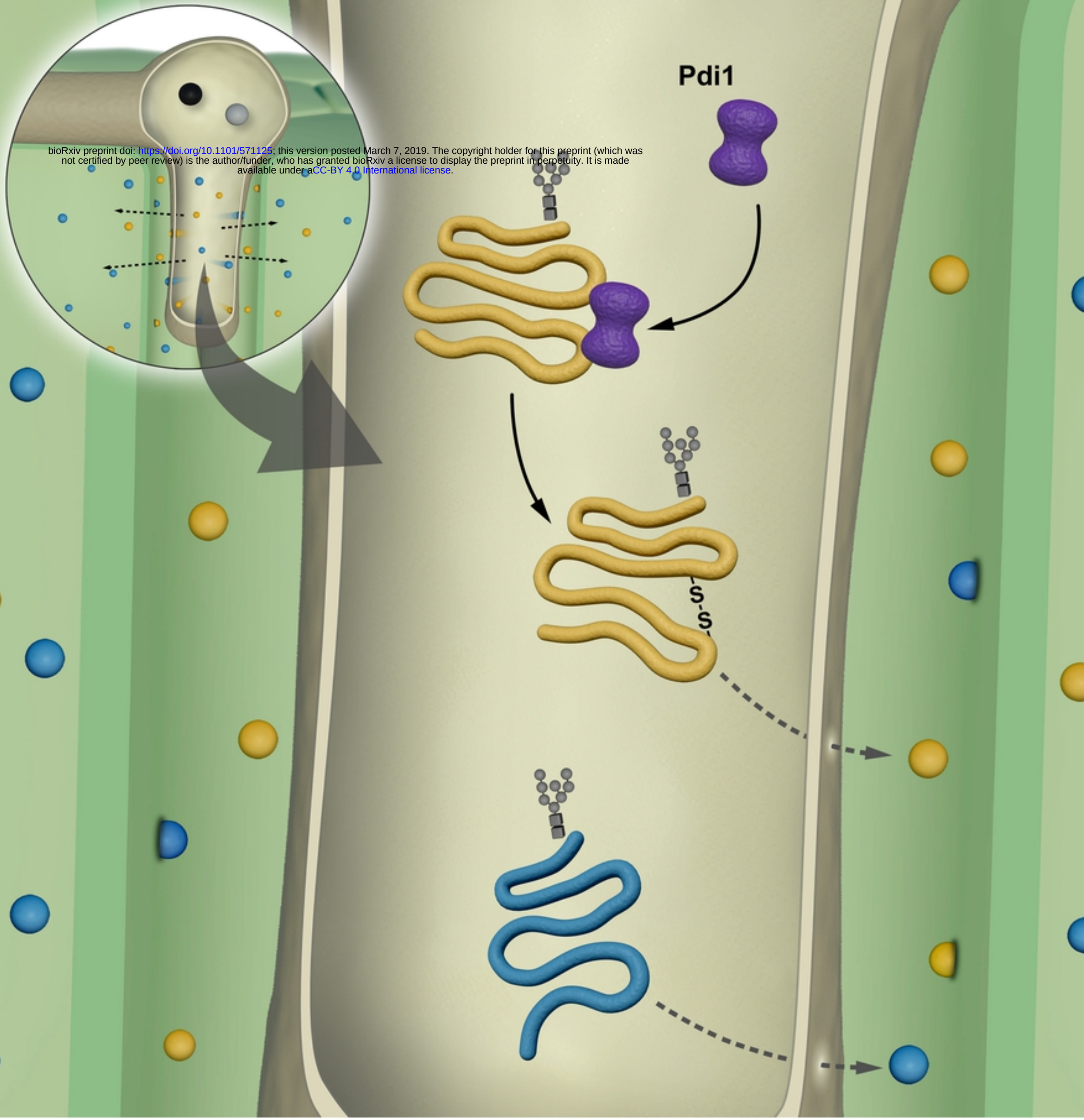


Figure 10

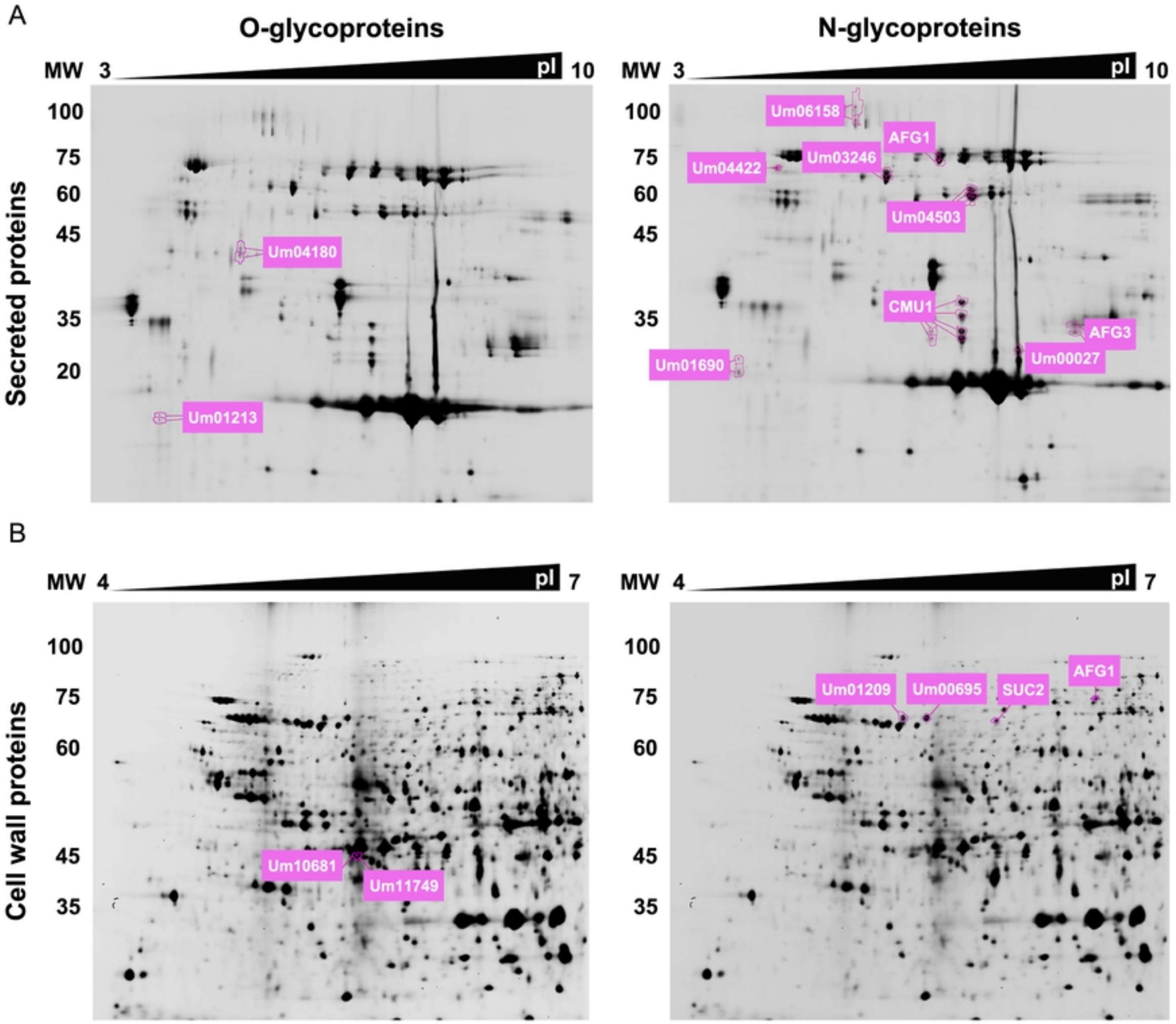


Figure 3

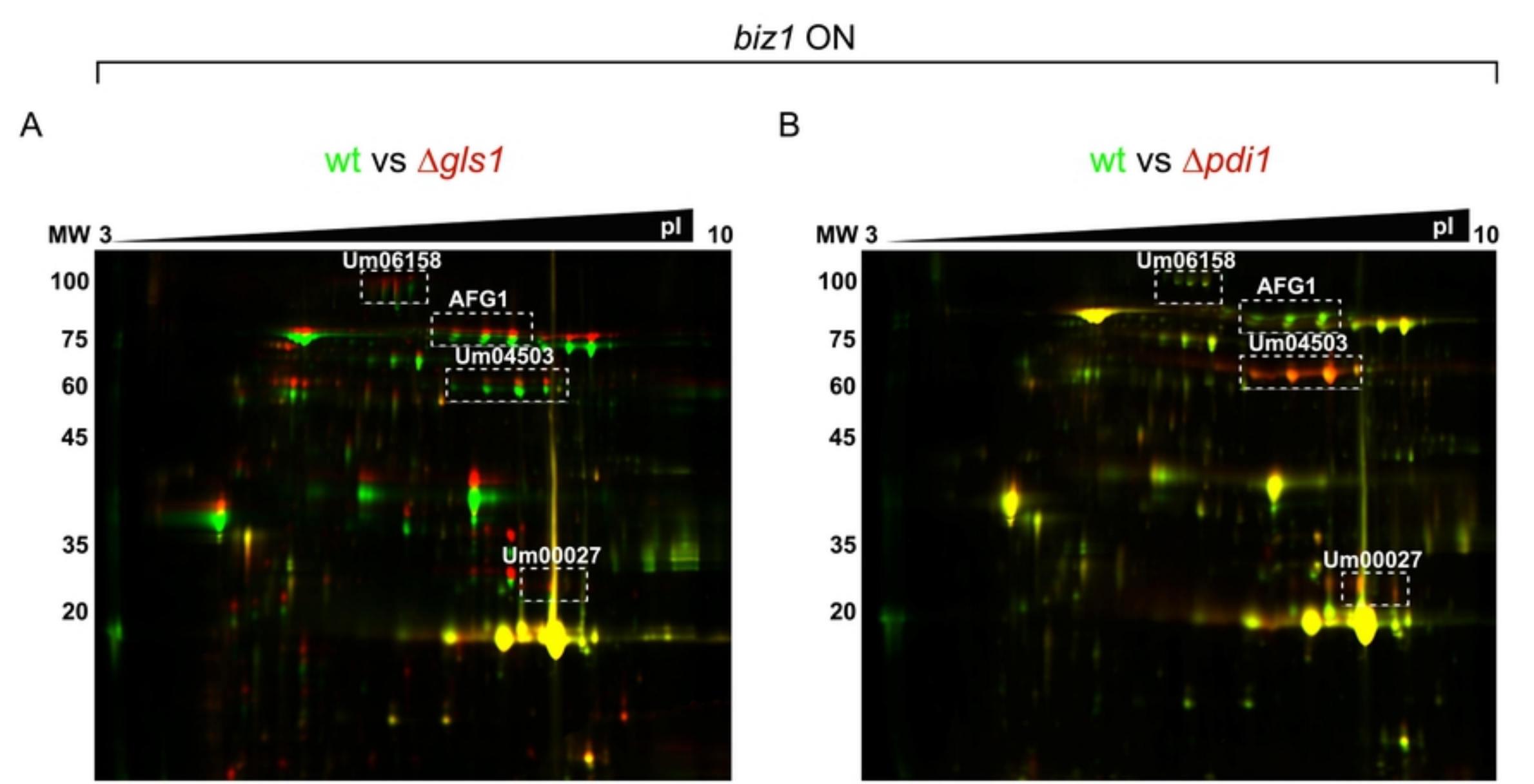
biz1 ON
A
wt vs Δgls1
MW 3
pI
10
100
75
60
45
35
20
Um06158
AFG1
Um04503
Um00027
B
wt vs Δpdi1
MW 3
pI
10
100
75
60
45
35
20
Um06158
AFG1
Um04503
Um00027

Figure 9